

Clustering of aerosol particles in isotropic turbulence

By JAEHUN CHUN¹, DONALD L. KOCH¹†,
SARMA L. RANI², ARUJ AHLUWALIA³
AND LANCE R. COLLINS²

¹School of Chemical and Biomolecular Engineering, Cornell University, Ithaca, NY 14853-5201, USA

²Sibley School of Mechanical and Aerospace Engineering, Cornell University,
Ithaca, NY 14853-7501, USA

³Epic Systems, 5301 Tokay Blvd, Madison, WI 53711, USA

(Received 2 May 2003 and in revised form 14 February 2005)

It has been recognized that particle inertia throws dense particles out of regions of high vorticity and leads to an accumulation of particles in the straining-flow regions of a turbulent flow field. However, recent direct numerical simulations (DNS) indicate that the tendency to cluster is evident even at particle separations smaller than the size of the smallest eddy. Indeed, the particle radial distribution function (RDF), an important measure of clustering, increases as an inverse power of the interparticle separation for separations much smaller than the Kolmogorov length scale. Motivated by this observation, we have developed an analytical theory to predict the RDF in a turbulent flow for particles with a small, but non-zero Stokes number. Here, the Stokes number (St) is the ratio of the particle's viscous relaxation time to the Kolmogorov time. The theory approximates the turbulent flow in a reference frame following an aerosol particle as a local linear flow field with a velocity gradient tensor and acceleration that vary stochastically in time. In monodisperse suspensions, the power-law dependence of the pair probability is seen to arise from a balance of an inward drift caused by the particles' inertia that scales linearly with the particle separation distance and a pairwise diffusion owing to the random nature of the flow with a diffusivity that scales quadratically with the particle separation distance. The combined effect leads to a power law behaviour for the RDF with an exponent, c_1 , that is proportional to St^2 . Predictions of the analytical theory are compared with two types of numerical simulation: (i) particle pairs interacting in a local linear flow whose velocity varies according to a stochastic velocity gradient model; (ii) particles interacting in a flow field obtained from DNS of isotropic turbulence. The agreement with both types of simulation is very good. The theory also predicts the RDF for unlike particle pairs (particle pairs with different Stokes numbers). In this case, a second diffusion process occurs owing to the difference in the response of the pair to local fluid accelerations. The acceleration diffusivity is independent of the pair separation distance; thus, the RDF of particles with even slightly different viscous relaxation times undergoes a transition from the power law behaviour at large separations to a constant value at sufficiently small separations. The radial separation corresponding to the transition between these two behaviours is predicted to be proportional to the difference between the Stokes numbers of the two particles. Once again, the agreement between the theory and simulations is found to be very good. Clustering of particles enhances their rate of coagulation or coalescence.

† Author to whom correspondence should be addressed.

The theory and linear flow simulations are used to obtain predictions for the rate of coagulation of particles in the absence of hydrodynamic and colloidal particle interactions.

1. Introduction

Many computational studies of aerosol particle motion in turbulent flows have shown that inertial particles are expelled from regions of high vorticity and preferentially concentrate in straining-flow regions (e.g. Maxey 1987; Squires & Eaton 1991; Eaton & Fessler 1994; McLaughlin 1994). An expected consequence of preferential concentration is that the probability of finding a pair of particles at separations comparable to the Kolmogorov length scale (the characteristic length scale of the strain and vorticity of a turbulent flow) is enhanced. However, Reade & Collins (2000*a*) showed that the radial distribution function (RDF), an important measure of clustering, grows as a power law of the inverse of the separation distance for separations much smaller than the Kolmogorov scale. Indeed, they were able to fit the RDF to a function of the form†

$$g(r) = c_0 \left(\frac{\eta}{r} \right)^{c_1}, \quad (1.1)$$

where $g(r)$ is the RDF, $\eta \equiv (\nu^3/\langle \epsilon \rangle)^{1/4}$ is the Kolmogorov length scale, $\langle \epsilon \rangle$ is the mean dissipation rate and ν is the kinematic viscosity. The existence of the power law for $r/\eta \approx 10^{-3}$ suggests there is more to the clustering phenomenon than the simple ejection of particles out of vortex cores.

These observations have important implications for the growth of particles by coagulation or coalescence. Turbulence-driven coagulation is an important mechanism governing the size distribution of aerosol particles with diameters in the range of about 1–20 μm . Smaller particles coagulate primarily owing to Brownian motion, while larger particles may coagulate or settle out owing to gravity. The rate of turbulent coagulation is proportional to the RDF evaluated at particle contact (Sundaram & Collins 1997; Wang, Wexler & Zhou 1998), which can grow in excess of 100 for certain parameter values (Reade & Collins 2000*a*). As the particle diameters of interest are typically much smaller than the Kolmogorov length scale (which is of order 50 μm to 1 mm), the sub-Kolmogorov-scale growth of the RDF can substantially increase the rate of coagulation.

In this paper, we analyse the mechanism responsible for the continued clustering of particles at sub-Kolmogorov length scales and develop an analytical theory to predict the power-law dependence of the RDF. The theory is derived for the limit of small particle inertia, where inertia is characterized by the particle Stokes number (see (2.5) for the definition). The approach is similar to those used by Balkovsky, Falkovich & Fouxon (2001) and Zaichik & Alipchenkov (2003), who independently derived relationships for the variance of the particle concentration. The predictions are compared extensively to two kinds of numerical simulations and in all cases there is very good agreement. The theory also explains the reduction in the RDF for

† Note that Reade & Collins (2000*a*) actually fit the pair correlation function defined as $h(r) \equiv g(r) - 1$; however, for $r/\eta \ll 1$ the two functions are nearly identical.

particles with different particle response times, as was observed in earlier numerical simulations (Reade & Collins 2000*b*; Zhou, Wexler & Wang 2001).

The outline of the paper is as follows. The mechanism for the sub-Kolmogorov clustering and the theory for the RDF is developed in §2. Section 3 summarizes the numerical methods used to simulate particle pairs in order to test the theory. Extensive comparisons between the results of the simulations and the predictions of the theory are presented in §4. We discuss the implications of our findings for coagulating systems in §5 and present conclusions in §6.

2. Theory

In this section, we will develop an analytical theory for the variation of the pair probability and RDF of both like and unlike particle pairs with radial separations r that are intermediate between the Kolmogorov scale and the particle diameter, i.e. $\eta \gg r \gg d$. The effects of hydrodynamic and colloidal interactions, finite particle size and coalescence events on the pair probability will be neglected. In general, these effects are expected to be negligible in a dilute suspension for $r \gg d$. For example, in non-inertial particle suspensions, coalescence-induced particle density variations are negligible if the particle volume fraction is much smaller than R_λ^{-1} where R_λ is the Reynolds number based on the Taylor microscale (Koch & Pope 2002).

Under these assumptions, the equations governing the motion of each of the suspended particles can be written as (Maxey & Riley 1983)

$$\frac{dx_i^{[j]}}{dt} = v_i^{[j]}, \quad (2.1a)$$

$$\frac{dv_i^{[j]}}{dt} = \frac{u_i(x_i^{[j]}) - v_i^{[j]}}{\tau_v^{[j]}}, \quad (2.1b)$$

where $x_i^{[j]}$, $v_i^{[j]}$, $\tau_v^{[j]} \equiv \rho_p^{[j]}(d^{[j]})^2/18\mu$, $\rho_p^{[j]}$ and $d^{[j]}$ are the position, velocity, viscous relaxation time, density and diameter of the j th particle, respectively, $u_i(x_i^{[j]})$ is the undisturbed fluid velocity at the particle centre and μ is the molecular viscosity of the fluid. If we put ourselves in the frame of reference moving with one of the particles, hereinafter designated as the *primary* particle (with a superscript $[p]$), and consider the relative motion of a neighbouring *satellite* particle (designated by a superscript $[s]$), we can derive the following equations for the relative position vector $\hat{r}_i \equiv x_i^{[s]} - x_i^{[p]}$ and relative velocity vector $\hat{w}_i \equiv v_i^{[s]} - v_i^{[p]}$

$$\frac{d\hat{r}_i}{dt} = \hat{w}_i, \quad (2.2a)$$

$$\frac{d\hat{w}_i}{dt} = \frac{\Gamma_{ij}^{[p]}\hat{r}_j - \hat{w}_i}{\tau_v^{[s]}} + a_i^{[p]} \left[\frac{\tau_v^{[p]}}{\tau_v^{[s]}} - 1 \right], \quad (2.2b)$$

where $\Gamma_{ij}^{[p]}$ and $a_i^{[p]}$ are the fluid velocity gradient and particle acceleration defined, respectively, as

$$\Gamma_{ij}^{[p]} \equiv \frac{\partial u_i}{\partial x_j}, \quad (2.3)$$

$$a_i^{[p]} \equiv \frac{dv_i^{[p]}}{dt}. \quad (2.4)$$

In deriving (2.2), we assume $\hat{r} \ll \eta$, allowing us to approximate the variation in the local fluid velocity as a linear function of position based on the velocity gradient, $\Gamma_{ij}^{[p]}(t)$, defined along the primary particle path. Notice that in addition to the effect of local shear, particle pairs with different response times will generate a relative velocity owing to the mismatch in the response of the two particles to acceleration. We will see that this plays an important role in the pair probability function for unlike particle pairs.

To investigate the origin of preferential concentration of small particles, we consider the motion of particles with $St \ll 1$, where the Stokes number is defined as

$$St^{[j]} \equiv \Gamma_\eta \tau_v^{[j]}, \quad (2.5)$$

$\Gamma_\eta \equiv \sqrt{\langle \epsilon \rangle} / \nu$ is the characteristic frequency for the smallest eddies, ϵ is the turbulent kinetic energy dissipation rate, ν is the kinematic viscosity of the gas and the angle brackets $\langle \cdot \rangle$ denote an ensemble average. The Stokes number being small translates to particle motions that are close to fluid particle trajectories. We can investigate this limit by performing a perturbation expansion in Stokes number of the particle-pair relative position and velocity. For the sake of simplicity, we first consider a monodisperse population of particles, and replace $St^{[j]}$ by St (we eventually will generalize the results for a polydisperse population, see §2.3). The perturbation expansions are shown below

$$\hat{r}_i = \hat{r}_i^{[0]} + St \hat{r}_i^{[1]} + St^2 \hat{r}_i^{[2]} + \dots, \quad (2.6a)$$

$$\hat{w}_i = \hat{w}_i^{[0]} + St \hat{w}_i^{[1]} + St^2 \hat{w}_i^{[2]} + \dots. \quad (2.6b)$$

Substituting these expressions into (2.2) and equating terms of equal order in St yields

$$\hat{w}_i^{[0]} = \hat{r}_j^{[0]} \Gamma_{ij}, \quad (2.7a)$$

$$\hat{w}_i^{[1]} = \hat{r}_j^{[1]} \Gamma_{ij} - \frac{\hat{r}_j^{[0]}}{\Gamma_\eta} \frac{d\Gamma_{ij}}{dt} - \frac{\hat{r}_k^{[0]}}{\Gamma_\eta} \Gamma_{kj} \Gamma_{ji}. \quad (2.7b)$$

Preferential concentration of particles at length scales smaller than the Kolmogorov scale can be attributed to a radial inward drift of inertial particles in the locally linear flow field. A definition of the drift velocity can be obtained from the above expressions by averaging the particle velocity at a specified radial location \mathbf{r} over an ensemble of particle tracks. If we restrict our attention to only those particles lying within an infinitesimal sphere centred at $\hat{\mathbf{r}} = \mathbf{r}$, then the conditioning implies to leading order

$$\hat{r}_i^{[0]} = r_i, \quad (2.8)$$

$$\hat{r}_i^{[1]} = 0. \quad (2.9)$$

The zeroth- and first-order contributions to the drift velocity are then, respectively,

$$\langle \hat{w}_i^{[0]} | \hat{r}_i = r_i \rangle_p = \langle \hat{r}_j^{[0]} \Gamma_{ij} \rangle_p = r_j \langle \Gamma_{ij} \rangle_p = 0, \quad (2.10)$$

$$\langle \hat{w}_i^{[1]} | \hat{r}_i = r_i \rangle_p = \left\langle \hat{r}_j^{[1]} \Gamma_{ij} - \frac{\hat{r}_j^{[0]}}{\Gamma_\eta} \frac{d\Gamma_{ij}}{dt} - \frac{\hat{r}_k^{[0]}}{\Gamma_\eta} \Gamma_{kj} \Gamma_{ji} \right\rangle_p = -\frac{r_k}{\Gamma_\eta} \langle \Gamma_{kj} \Gamma_{ji} \rangle_p, \quad (2.11)$$

where $\langle \cdot \rangle_p$ denotes the average over an ensemble of primary particle trajectories. The zeroth-order term is identically zero owing to isotropy. The first and second terms on the right-hand side of (2.11) are zero owing to (2.9) and stationarity, respectively; however, the third term is not zero for finite-Stokes-number particles. Tensorial constraints

for an isotropic system allow us to simplify the velocity gradient correlation as shown below

$$\langle \Gamma_{kj} \Gamma_{ji} \rangle_p = \frac{1}{3} \langle \Gamma_{lj} \Gamma_{jl} \rangle_p \delta_{ki}. \quad (2.12)$$

Defining the rate of strain and rate of rotation tensors, respectively, as

$$S_{ij} \equiv \frac{1}{2}(\Gamma_{ij} + \Gamma_{ji}), \quad (2.13a)$$

$$R_{ij} \equiv \frac{1}{2}(\Gamma_{ij} - \Gamma_{ji}), \quad (2.13b)$$

allows us to re-express $\Gamma_{lj} \Gamma_{jl}$ as

$$\begin{aligned} \Gamma_{lj} \Gamma_{jl} &= (S_{lj} + R_{lj})(S_{jl} + R_{jl}) \\ &= (S_{lj} + R_{lj})(S_{lj} - R_{lj}) \\ &= S_{lj} S_{lj} - R_{lj} R_{lj} \\ &= S^2 - R^2, \end{aligned} \quad (2.14)$$

where $S^2 \equiv S_{ij} S_{ij}$ and $R^2 \equiv R_{ij} R_{ij}$ are the second invariant of the rate of strain and rate of rotation tensors, respectively. Substituting this relationship into (2.11) yields the mean drift velocity

$$\langle \hat{w}_i | \hat{r}_i = r_i \rangle_p = -A \Gamma_{\eta} r_i, \quad (2.15)$$

where the non-dimensional coefficient A is defined as

$$A \equiv \frac{St}{3\Gamma_{\eta}^2} [\langle S^2 \rangle_p - \langle R^2 \rangle_p]. \quad (2.16)$$

Notice that the drift velocity is always parallel to the separation vector and is proportional to St and hence is zero for fluid particles. Secondly, the quantity $[\langle S^2 \rangle_p - \langle R^2 \rangle_p]$ is also zero for a fluid particle because a fluid particle samples equal amounts of strain and rotation; however, an inertial particle samples more strain than rotation and hence generates a net inward drift velocity. Equation (2.15) is valid until other effects (e.g. hydrodynamic interactions, excluded volume or possibly coalescence) modify the particle motions at separations of the order $r = O(d)$.

The above analysis is useful because it provides a simple physical explanation and model for the inward flux of finite-inertia particles. However, it introduces correlations that are not readily determined from experiments (statistics measured along finite-Stokes-number particle tracks) and does not include the effect of turbulent diffusion. In order to derive a closed expression for the RDF that accounts for drift and diffusion, a conservation law based on probabilistic arguments is required.

2.1. Probability analysis of particle pair separations

There are two shortcomings to (2.15): first, we cannot easily determine $[\langle S^2 \rangle_p - \langle R^2 \rangle_p]$ and so, as of yet, we cannot compute the drift velocity; and secondly, randomness of $\Gamma_{ij}^{[p]}(t)$ acting on gradients of probability will give rise to a diffusive flux that opposes and eventually comes into balance with the drift. In this section, we analyse the probability of pair separations in a manner that incorporates both the drift and diffusion of the pair. We will develop statistical arguments for Lagrangian trajectories following a fluid path (not a particle path), based on the assumption that the two are very nearly the same in the limit $St \ll 1$. In this way, the statistical inputs to the theory will only involve fluid properties (i.e. particle-path averages will not be required). In deriving the drift and diffusion terms, we seek only the leading-order contribution (in the perturbation expansion in St).

In the frame of reference moving with a primary particle, we define the conditional probability of finding a second particle separated by the vector \mathbf{r} as

$$P(r_i, t | \Gamma_{ij}(t)) \equiv \overline{\delta(\hat{r}_i - r_i)}, \quad (2.17)$$

where the overbar signifies an ensemble average over the set of initial conditions for the satellite particles.† Note that the history for the velocity gradient along the primary particle path, $\Gamma_{ij}(t)$, is considered known and fixed in this representation. In addition, we do not consider the joint distribution of position and velocity as is sometimes done (e.g. Koch 1990; Reeks 1991), under the assumption that $St \ll 1$ implies the particle motion is very closely tied to the fluid and, to leading order, completely specified by the particle position and the velocity gradient. Under these assumptions, the closed deterministic evolution equation for $P(r_i, t | \Gamma_{ij}(t))$ can be written as (see, for example, Appendix J in Pope 2000)

$$\frac{\partial P}{\partial t} + \frac{\partial W_i P}{\partial r_i} = 0, \quad (2.18)$$

where we have suppressed the arguments for P and

$$W_i(\mathbf{r}) \equiv \overline{\hat{w}_i \delta(\hat{r}_i - r_i) / \delta(\hat{r}_i - r_i)}. \quad (2.19)$$

The RDF for an isotropic system, $g(r)$, is related to the ensemble average of the pair probability by (e.g. see Reade & Collins 2000a)

$$g(r) = \frac{N(N-1)}{n^2 V} \langle P \rangle(r), \quad (2.20)$$

where N is the total number of particles lying within the control volume V , $n \equiv N/V$ is the number density of particles, and the averaging implied by $\langle \cdot \rangle$ is over an ensemble of primary particle trajectories that are statistically equivalent. The above normalization ensures that $g(r)$ is dimensionless and approximately equal to unity for a uniform distribution of particles. Whereas (2.18) is a closed equation, the equation for $g(r)$ (or equivalently for $\langle P \rangle(r)$) will not be, owing to the coupling of fluctuations in the relative velocity W_i with P .

Averaging (2.18) yields

$$\frac{\partial \langle P \rangle}{\partial t} + \frac{\partial}{\partial r_i} (\langle W_i \rangle \langle P \rangle + \langle W_i P' \rangle) = 0, \quad (2.21)$$

where $P' \equiv P - \langle P \rangle$. $\langle W_i \rangle$ represents the mean relative velocity experienced by pairs that sample the fluid flow uniformly. This quantity is zero because, as shown in (2.15) and (2.16), the mean drift is proportional to the difference in mean strain and rotation experienced along a primary particle trajectory, which is zero for a fluid particle in stationary isotropic turbulence. Thus, drift in this representation arises from the coupling of fluctuations in the probability with fluctuations in the relative velocity. To close (2.21), we must approximate the fluctuation in the pair probability, P' . An equation for P' can be obtained by substituting $P = \langle P \rangle + P'$ into (2.18)

$$\frac{\partial P'}{\partial t} + \frac{\partial}{\partial r_i} (W_i P') = -\frac{\partial}{\partial r_i} (W_i \langle P \rangle) - \frac{\partial \langle P \rangle}{\partial t}. \quad (2.22)$$

It will be verified *a posteriori* that the average probability evolves over a time scale $\ln(\eta/r)/\Gamma_\eta$ so that $\partial \langle P \rangle / \partial t$ is $O(1/\ln(\eta/r))$ smaller than $(\partial/\partial r_i)(W_i \langle P \rangle)$ and will be

† This average is to be distinguished from $\langle \cdot \rangle$, which is an ensemble average over primary particle trajectories.

neglected. Equation (2.22) may then be solved using the method of characteristics to yield

$$P'(\mathbf{r}, t) = - \int_{-\infty}^t dt' \frac{\partial}{\partial r_i} [W_i(\mathbf{r}', t') \langle P \rangle(\mathbf{r}', t')], \quad (2.23)$$

where \mathbf{r}' is a characteristic variable that satisfies the ordinary differential equation

$$\frac{\partial r'_i}{\partial t'} = W_i(\mathbf{r}', t'), \quad (2.24)$$

and boundary condition

$$r'_i = r_i \text{ at } t' = t. \quad (2.25)$$

Substituting (2.23) into (2.21) yields a closed equation for the average pair distribution function

$$\frac{\partial \langle P \rangle}{\partial t} + \frac{\partial}{\partial r_i} (q_i^d + q_i^D) = 0, \quad (2.26)$$

that includes a drift flux

$$q_i^d(\mathbf{r}) = - \int_{-\infty}^t \left\langle W_i(\mathbf{r}, t) \frac{\partial W_l}{\partial r'_l}(\mathbf{r}', t') \right\rangle \langle P \rangle(\mathbf{r}', t') dt', \quad (2.27)$$

and a shear diffusive flux

$$q_i^D(\mathbf{r}) = - \int_{-\infty}^t \langle W_i(\mathbf{r}, t) W_j(\mathbf{r}', t') \rangle \frac{\partial \langle P \rangle}{\partial r'_j}(\mathbf{r}', t') dt'. \quad (2.28)$$

Equation (2.26) is non-local in the sense that the flux at \mathbf{r} depends on the pair probability and its derivative at other pair separations \mathbf{r}' . We discuss the modelling of the drift and diffusion fluxes in the subsections below.

2.1.1. Drift flux

It is possible to derive a closed expression for the drift flux, $q_i^d(\mathbf{r})$. We begin by first recalling that the radial velocity for satellite particles in the limit $St \ll 1$ can be approximated as

$$W_i(\mathbf{r}) = r_k \Gamma_{ik} + \frac{St}{\Gamma_\eta} r_k \Gamma_{kj} \Gamma_{ji} + \dots \quad (2.29)$$

The divergence of this velocity is then

$$\frac{\partial W_l}{\partial r_l} = \Gamma_{ll} + \frac{St}{\Gamma_\eta} \Gamma_{lm} \Gamma_{ml} + \dots = \frac{St}{\Gamma_\eta} \Gamma_{lm} \Gamma_{ml}. \quad (2.30)$$

The first term on the right-hand side is zero owing to continuity. The dominant contributions to the integral in (2.27) come from the time interval $t - t' = O(1/\Gamma_\eta)$, for which the turbulent velocity gradient retains correlation. It will be seen from the solution for the RDF (which is proportional to the pair probability) given in (2.72) and (2.75) that $\langle P \rangle(\mathbf{r}') = \langle P \rangle(\mathbf{r}) [1 + O(St^2)]$ over this time interval. Approximating $\langle P \rangle(\mathbf{r}') \approx \langle P \rangle(\mathbf{r})$ and using (2.29) and (2.30), we can express the drift flux as follows

$$q_i^d(\mathbf{r}) = - \langle P \rangle(\mathbf{r}) r_k \int_{-\infty}^t \left[\frac{St}{\Gamma_\eta} \langle \Gamma_{ik}(t) \Gamma_{lm}(t') \Gamma_{ml}(t') \rangle + \frac{St^2}{\Gamma_\eta} \langle \Gamma_{kj}(t) \Gamma_{ji}(t) \Gamma_{lm}(t') \Gamma_{ml}(t') \rangle \right] dt'. \quad (2.31)$$

Tensor constraints for an isotropic system require

$$\begin{aligned} \langle \Gamma_{ik}(t) \Gamma_{lm}(t') \Gamma_{ml}(t') \rangle &= \frac{1}{3} \delta_{ik} \langle \Gamma_{nn}(t) \Gamma_{lm}(t') \Gamma_{ml}(t') \rangle = 0, \\ \langle \Gamma_{kj}(t) \Gamma_{ji}(t) \Gamma_{lm}(t') \Gamma_{ml}(t') \rangle &= \frac{1}{3} \delta_{ik} \langle \Gamma_{nj}(t) \Gamma_{jn}(t) \Gamma_{lm}(t') \Gamma_{ml}(t') \rangle. \end{aligned}$$

By taking advantage of (2.14), we have

$$\langle \Gamma_{kj}(t)\Gamma_{ji}(t)\Gamma_{lm}(t')\Gamma_{ml}(t') \rangle = \frac{1}{3}\delta_{ik}\langle [S^2(t) - R^2(t)][S^2(t') - R^2(t')] \rangle.$$

Substituting this relationship into (2.31) yields

$$q_i^d(\mathbf{r}) = -A\Gamma_\eta r_i \langle P \rangle(\mathbf{r}), \tag{2.32}$$

where the non-dimensional coefficient A is given by

$$A = \frac{St^2}{3\Gamma_\eta} \int_{-\infty}^t \langle [S^2(t) - R^2(t)][S^2(t') - R^2(t')] \rangle dt'. \tag{2.33}$$

To put this expression into a more standard form, we introduce the relationships

$$S^2(t) \equiv \frac{\epsilon(t)}{2\nu}, \tag{2.34a}$$

$$R^2(t) \equiv \frac{\zeta(t)}{2\nu}, \tag{2.34b}$$

where $\epsilon(t)$ is the instantaneous kinetic energy dissipation rate and $\zeta(t)$ is the instantaneous enstrophy (square of the vorticity) times the kinematic viscosity. Substituting this above yields

$$A = \frac{St^2}{12\nu^2\Gamma_\eta} \int_{-\infty}^t \langle [\epsilon(t) - \zeta(t)][\epsilon(t') - \zeta(t')] \rangle dt'. \tag{2.35}$$

The means of $\langle \epsilon \rangle$ and $\langle \zeta \rangle$ are equal by definition and therefore cancel out in (2.35). Contributions from the fluctuations $\epsilon'(t)$ and $\zeta'(t)$ can be written in terms of integral time correlations as shown below

$$A = \frac{1}{12}St^2[\sigma_\epsilon^2 T_{\epsilon\epsilon} - \rho_{\epsilon\zeta}\sigma_\epsilon\sigma_\zeta(T_{\epsilon\zeta} + T_{\zeta\epsilon}) + \sigma_\zeta^2 T_{\zeta\zeta}], \tag{2.36}$$

where σ_X is the standard deviation of the variable X normalized by its mean $\langle X \rangle$, ρ_{XY} is the cross-correlation coefficient, defined as

$$\rho_{XY} = \frac{\langle (X - \langle X \rangle)(Y - \langle Y \rangle) \rangle}{\sqrt{\langle (X - \langle X \rangle)^2 \rangle \langle (Y - \langle Y \rangle)^2 \rangle}}, \tag{2.37}$$

and T_{XY} is the normalized correlation time defined as

$$T_{XY} \equiv \frac{\Gamma_\eta \int_0^\infty \langle (X(0) - \langle X \rangle)(Y(t) - \langle Y \rangle) \rangle dt}{\langle (X - \langle X \rangle)(Y - \langle Y \rangle) \rangle}. \tag{2.38}$$

If we compare (2.36) with the expression derived previously based on particle-track averages (2.16), we can surmise the following relationships for $\langle S^2 \rangle_p$ and $\langle R^2 \rangle_p$

$$\langle S^2 \rangle_p = \frac{1}{2}\Gamma_\eta^2 \left[1 + \frac{1}{2}St(\sigma_\epsilon^2 T_{\epsilon\epsilon} - \rho_{\epsilon\zeta}\sigma_\epsilon\sigma_\zeta T_{\zeta\epsilon}) \right], \tag{2.39a}$$

$$\langle R^2 \rangle_p = \frac{1}{2}\Gamma_\eta^2 \left[1 + \frac{1}{2}St(\rho_{\epsilon\zeta}\sigma_\epsilon\sigma_\zeta T_{\epsilon\zeta} - \sigma_\zeta^2 T_{\zeta\zeta}) \right]. \tag{2.39b}$$

We conclude that $[\langle S^2 \rangle_p - \langle R^2 \rangle_p]$ is proportional to St in the limit $St \ll 1$.

2.1.2. Local diffusion flux

Next we consider the turbulent diffusion process. Before considering the non-local analysis applicable to a turbulent flow, we will briefly review the treatment by Brunk, Koch & Lion (1997) of local pair diffusion that occurs in a stochastic flow in which

the characteristic correlated strain and rotation are small, i.e. $\Gamma_\eta \tau_S \ll 1$ and $\Gamma_\eta \tau_R \ll 1$. Here, τ_S and τ_R are the autocorrelation times of components of the strain and rotation, respectively. When the correlated strain is small, $\mathbf{r}' \approx \mathbf{r}$ so the non-local diffusion flux shown in (2.28) can be approximated by the local diffusion flux

$$q_i^D(\mathbf{r}) = -\mathcal{D}_{ij}(\mathbf{r}) \frac{\partial \langle P \rangle}{\partial r_j}, \quad (2.40)$$

where the turbulent diffusivity, \mathcal{D}_{ij} is defined as

$$\mathcal{D}_{ij}(\mathbf{r}) = \int_{-\infty}^t \langle W_i(t) W_j(t') \rangle dt'. \quad (2.41)$$

To leading order, \mathcal{D}_{ij} is independent of the particle Stokes number, and therefore fluid particle velocities can be substituted into (2.41) yielding

$$\mathcal{D}_{ij}(\mathbf{r}) = \int_{-\infty}^t \langle \hat{r}_m(t) \Gamma_{im}(t) \hat{r}_n(t') \Gamma_{jn}(t') | \hat{r}_i = r_i \rangle dt'.$$

Additionally, the local analysis neglects the change in the radial position of the satellite particle over a correlation time for the velocity gradient, allowing us to simplify the expression further

$$\mathcal{D}_{ij}(\mathbf{r}) = r_m r_n \int_{-\infty}^t \langle \Gamma_{im}(t) \Gamma_{jn}(t') \rangle dt'. \quad (2.42)$$

Making the substitutions $\Gamma_{im}(t) = [S_{im}(t) + R_{im}(t)]$ and $\Gamma_{jn}(t') = [S_{jn}(t') + R_{jn}(t')]$ yields

$$\mathcal{D}_{ij}(\mathbf{r}) = r_m r_n \int_{-\infty}^t \langle [S_{im}(t) + R_{im}(t)][S_{jn}(t') + R_{jn}(t')] \rangle dt'.$$

Brunk *et al.* (1997) evaluated this expression for an isotropic random field assuming the time correlations for strain and rotation, τ_S and τ_R respectively, are known. The result is

$$\mathcal{D}_{ij}(\mathbf{r}) = r_m r_n \Gamma_\eta^2 [\tau_S S_{imjn} + \tau_R R_{imjn}], \quad (2.43)$$

where

$$S_{imjn} \equiv \frac{1}{20} [\delta_{ij} \delta_{mn} + \delta_{in} \delta_{mj} - \frac{2}{3} \delta_{im} \delta_{jn}], \quad (2.44a)$$

$$R_{imjn} \equiv \frac{1}{12} [\delta_{ij} \delta_{mn} - \delta_{in} \delta_{mj}]. \quad (2.44b)$$

Substituting (2.44) into (2.43) and simplifying yields

$$\mathcal{D}_{ij}(\mathbf{r}) = \frac{\Gamma_\eta^2 r^2}{60} \left[(3\tau_S + 5\tau_R) \delta_{ij} + (\tau_S - 5\tau_R) \frac{r_i r_j}{r^2} \right]. \quad (2.45)$$

For an isotropic system we can express the general diffusivity tensor as (Hinze 1975)

$$\mathcal{D}_{ij}(\mathbf{r}) = \mathcal{D}_{\perp\perp}(r) \delta_{ij} + [\mathcal{D}_{\parallel\parallel}(r) - \mathcal{D}_{\perp\perp}(r)] \frac{r_i r_j}{r^2}, \quad (2.46)$$

where $\mathcal{D}_{\parallel\parallel}(r)$ and $\mathcal{D}_{\perp\perp}(r)$ are, respectively, the components of the diffusivity parallel and perpendicular to the separation vector, \mathbf{r} . As already noted, we are interested only in the radial component of the diffusion flux (as the drift flux is only in this direction), defined as

$$q_r^D(r) = -\mathcal{D}_{\parallel\parallel}(r) \frac{\partial \langle P \rangle}{\partial r}. \quad (2.47)$$

By comparing (2.45) with (2.46) we arrive at the final expression for $\mathcal{D}_{\parallel}(r)$

$$\mathcal{D}_{\parallel}(r) = B_l \Gamma_{\eta} r^2, \quad (2.48)$$

where the dimensionless coefficient B_l is given by

$$B_l \equiv \frac{1}{15} \Gamma_{\eta} \tau_S. \quad (2.49)$$

The subscript ‘ l ’ refers to the fact that this is a local analysis that neglects the change in the position of the satellite particle that occurs over a characteristic correlation time for the strain.

2.1.3. Non-local diffusion flux

As noted in Brunk *et al.* (1998), the local description of diffusion given in (2.48) and (2.49) is applicable only for a stochastic linear flow field in which $\tau_S \Gamma_{\eta} \ll 1$. Direct numerical simulations of incompressible, Newtonian turbulence (Yeung & Pope 1989) have shown that $\tau_S \Gamma_{\eta} \approx 2.3$ and hence the straining field persists for a sufficient period of time that particle pairs are transported through distances comparable with their initial separation. Across these distances, substantial changes in $\partial \langle P \rangle / \partial r$ occur. This suggests the need for a non-local description of the diffusive flux, in which the diffusive flux in one radial position is influenced by the pair probability (or its gradient) at other radial positions, leading to an integro-differential equation for the mean pair probability.

Obtaining a closed expression for a general turbulent flow field is not feasible. Instead, we adopt a simple description of the turbulent flow to model the non-local diffusion process. First, we assume that the straining and rotating motions act independently in altering the pair’s relative position. Consequently, the rotational motion only affects the angular position of the pair and not their radial separation, and so can be neglected. Brunk *et al.* (1998) observed that rotational motions have a small effect on the coagulation rate in isotropic turbulence, supporting this supposition. The strain component of the turbulence is then assumed to consist of a random sequence of uniaxial extensional or compressional flows defined by

$$S_{ij} = \pm \frac{\Gamma_{\eta}}{\sqrt{3} f_s} [e_i e_j - \frac{1}{2}(\delta_{ij} - e_i e_j)], \quad (2.50)$$

where e_i is a randomly chosen unit vector and the flow is uniaxial extension or compression (equivalently biaxial extension) depending upon the sign in (2.50).

We define f_s as the fraction of time that a flow is occurring, and f_+ and $f_- \equiv 1 - f_+$ as the fraction of those flows that are extensional (corresponding to the + sign) and compressional (corresponding to the – sign), respectively. We set $f_s = 27/10 \pi = 0.859$ in order to reproduce the Saffman & Turner (1956) formula for the coagulation rate in the limit $\Gamma_{\eta} \tau_S \rightarrow \infty$. The fraction of the straining motions that are uniaxial extension is chosen to be $f_+ = 0.188$ to reproduce the third invariant of the strain tensor, $\langle S_{ij} S_{jk} S_{ki} \rangle = -0.113 \Gamma_{\eta}^3$, obtained from DNS of isotropic turbulence (Girimaji & Pope (1990)). The strong preference for uniaxial compression over extension is connected to the well-known skewness in the velocity derivatives that is responsible for energy transfer (Cantwell 1993). To obtain a strain rate correlation function that decays exponentially with a characteristic time scale τ_S , we set the probability density function for the lifetime of each event, t_f , to be

$$F(t_f) = \frac{f_s t_f}{\tau_S^2} \exp\left(-\frac{t_f}{\tau_S}\right). \quad (2.51)$$

Given this simple prescription of the local velocity gradient, it is possible to calculate the radial flux of particles crossing a spherical surface of radius r

$$4\pi r^2 q_r^D(r) = \int d\Omega \int_0^\infty dt_f F(t_f) \int_0^\infty dr_0 4\pi r_0^2 \langle P \rangle(r_0) [f_+ I_+(r, r_0, r_{f+}) + f_- I_-(r, r_0, r_{f-})], \quad (2.52)$$

where $d\Omega$ is the differential solid angle for the axis of symmetry of the straining motion, r_0 is the initial separation distance of the particle pair before the straining event, $r_{f\pm}$ is the final separation distance after the straining event, and I_\pm is an indicator function with the definition

$$I_\pm \equiv \begin{cases} +1 & \text{particle leaves sphere,} \\ -1 & \text{particle enters sphere,} \\ 0 & \text{otherwise.} \end{cases} \quad (2.53)$$

Note that the subscript \pm refers back to the sign in (2.50). The indicator function is used to count the net loss of particles from within the sphere over the duration of an event. In order to develop a mathematical expression for I , we must determine the initial and final position of each pair of particles. It is convenient to define a non-dimensional initial particle location as $R_0 \equiv r_0/r$. To determine the fate of that particle pair following the straining motion, we need an expression for the trajectory. An important advantage of assuming uniaxial extension or compression is that the trajectories can be evaluated analytically. For example, the non-dimensional final position of a particle pair with an initial position of R_0 can be written as

$$R_{f+} = R_0 \left[\mu^2 \theta^2 + \frac{(1 - \mu^2)}{\theta} \right]^{-1/2}, \quad (2.54)$$

$$R_{f-} = R_0 \left[\frac{\mu^2}{\theta^2} + (1 - \mu^2)\theta \right]^{-1/2}, \quad (2.55)$$

for uniaxial extension (2.54) and compression (2.55), respectively, where μ is the cosine of the angle between the axis of symmetry of the straining motion and the separation vector of the particle pair, and

$$\theta \equiv \exp\left(\frac{\Gamma_\eta t_f}{\sqrt{3} f_s}\right). \quad (2.56)$$

We now can write down a simple expression for the indicator function

$$I_\pm(R_0, \mu, t_f) = H(1 - R_0)H(R_{f\pm} - 1) - H(R_0 - 1)H(1 - R_{f\pm}), \quad (2.57)$$

where $H(x)$ is the Heaviside function, defined to be zero for negative arguments x and unity for positive arguments x .

It can be shown that the power-law pair probability of the form given in (1.1) is a steady-state solution to the conservation equation for the pair probability, (2.26), with (2.15) and (2.52) for the drift and non-local diffusion fluxes, respectively. Substituting (1.1) for the pair probability in (2.52) yields

$$q_r^D(r) = -B_{nl} \Gamma_\eta r^2 \frac{\partial \langle P \rangle}{\partial r}, \quad (2.58)$$

which is identical to (2.47)–(2.49), except that the non-local coefficient, B_{nl} , is defined as

$$B_{nl} = \Gamma_\eta^{-1} \int d\Omega \int_0^\infty dt_f F(t_f) \int_0^\infty dR_0 R_0^{2-c_1} [f_+ I_+(R_0, \mu, t_f) + f_- I_-(R_0, \mu, t_f)]. \quad (2.59)$$

In the limit $St \ll 1$, the pair probability power law exponent c_1 will be asymptotically small. Expanding (2.59) for small c_1 yields to leading order

$$B_{nl} = 0.0926. \quad (2.60)$$

Thus, provided that $\langle P \rangle$ is a power law, the non-local diffusion flux at steady state has the same functional form as the diffusion flux based on the local diffusion approximation; however, the resulting coefficient is approximately 40 % smaller than the value that would have been obtained by extrapolating the local diffusion expression (2.49) to $\Gamma_\eta \tau_S = 2.3$. In the subsequent analysis, we will use the gradient closure shown in (2.58) with (2.60) as the coefficient.

2.1.4. Diffusion due to turbulent accelerations

Recall that (2.2) has an additional term that exists whenever the primary and satellite particles have different relaxation times. The resulting relative velocity gives rise to an additional diffusion process for the particle pair. In the limit where both $St^{[p]} \ll 1$ and $St^{[s]} \ll 1$, we can express the relative velocity to leading order as

$$W_i = (St^{[p]} - St^{[s]}) \frac{a_i}{\Gamma_\eta}, \quad (2.61)$$

where a_i is the acceleration of the fluid element located at the centre of the primary particle. If the relative displacement of the particle pair over the characteristic correlation time for acceleration, τ_a , is much smaller than the particle separation, r , then the fluctuating velocity induced by the turbulent accelerations will give rise to a local diffusive flux of the form

$$q_i^a(\mathbf{r}) = -\mathcal{D}_{ij}^a \frac{\partial \langle P \rangle}{\partial r_j}, \quad (2.62)$$

with a diffusivity defined as

$$\mathcal{D}_{ij}^a = \int_{-\infty}^t \langle W_i(t) W_j(t') \rangle dt'. \quad (2.63)$$

Substituting (2.61) into (2.63) yields

$$\mathcal{D}_{ij}^a = \frac{(St^{[p]} - St^{[s]})^2}{\Gamma_\eta^2} \int_{-\infty}^t \langle a_i(t) a_j(t') \rangle dt'. \quad (2.64)$$

We can express this in terms of the statistics of acceleration as shown below

$$\mathcal{D}_{ij}^a = \frac{(St^{[p]} - St^{[s]})^2}{3\Gamma_\eta^2} \sigma_a^2 \tau_a \delta_{ij}. \quad (2.65)$$

Based on Kolmogorov-type scaling, the acceleration variance is usually written as (e.g. Yeung & Pope 1989)

$$\langle a^2 \rangle = \sigma_a^2 = a_0 \eta^2 \Gamma_\eta^4, \quad (2.66)$$

where according to the original Kolmogorov argument a_0 is expected to be a universal constant, but has been found to be a function of Reynolds number in recent DNS

and experiments (Yeung 2001; Voth *et al.* 2002). Substituting this into (2.65) yields

$$\mathcal{D}_{ij}^a = \frac{(St^{[pl]} - St^{[sl]})^2}{3} a_0 \eta^2 \Gamma_\eta^2 \tau_a \delta_{ij}. \quad (2.67)$$

Evaluating the radial component of the flux yields

$$q_r^a(r) = -\mathcal{D}_{||}^{[a]} \frac{\partial \langle P \rangle}{\partial r}, \quad (2.68)$$

where $\mathcal{D}_{||}^a$ for an isotropic system is given by

$$\mathcal{D}_{||}^a = (St^{[pl]} - St^{[sl]})^2 a_0 \eta^2 \Gamma_\eta^2 \tau_a. \quad (2.69)$$

One complication with this formula is that the acceleration correlation $\langle a_i(t)a_i(t') \rangle$ becomes negative for $\Gamma_\eta |t - t'| > 3$, and in fact integrates to zero for stationary turbulence. This issue was circumvented by Yeung (2001), who defined the correlation time as the time when the correlation function crossed the zero axis. Here, we replace this definition by fitting the early-time behaviour of the correlation to an exponential of the form

$$\langle a_i(t)a_i(t') \rangle = \exp\left(-\frac{|t - t'|}{\tau_a}\right). \quad (2.70)$$

The physical justification for this assumption is that the particles are influenced mainly by the initial stages of an acceleration event. The small negative tail of the acceleration correlation has little influence because it ensues only at long times after the particle pair has reoriented. Curve fits of the DNS used in this study yielded (for $R_\lambda = 47.1$) $a_0 = 1.545$ and $\tau_a = 1.5/\Gamma_\eta$.

2.2. Monodisperse RDF

The previous relationships for the drift flux (see (2.32) and (2.36)) and non-local diffusion flux (see (2.58) and (2.60)) can be substituted into the conservation equation for mean probability (2.26) and renormalized according to the definition of the RDF given in (2.20) to produce a closed expression for the RDF of a monodisperse collection of particles in isotropic turbulence

$$\frac{\partial g(r, t)}{\partial t} = \frac{1}{r^2} \frac{\partial [r^2 \text{Arg}(r, t)]}{\partial r} + \frac{1}{r^2} \frac{\partial}{\partial r} \left[r^2 B_{nl} r^2 \frac{\partial g(r, t)}{\partial r} \right]. \quad (2.71)$$

The steady-state solution to (2.71), assuming no net drift of particles from infinity, is

$$g(r, \infty) = c_0 \left(\frac{\eta}{r} \right)^{c_1}, \quad (2.72)$$

where c_0 is an unspecified matching coefficient and

$$c_1 = \frac{A}{B_{nl}}. \quad (2.73)$$

Note that the analysis we have performed cannot determine the value of c_0 , since we have considered only the locally linear flow that is valid for $r \ll \eta$. The value of c_0 depends upon the manner in which the locally linear flow transitions to full turbulence at larger separations, which is beyond the scope of this study.

Based on our earlier findings, we can express c_1 in two forms: one uses (2.15) and (2.16) to express the power in terms of $[\langle S^2 \rangle_p - \langle R^2 \rangle_p]$

$$c_1 = 3.61 \frac{St}{\Gamma_\eta^2} [\langle S^2 \rangle_p - \langle R^2 \rangle_p], \quad (2.74)$$

and the second uses the relationship for A given in (2.36)

$$c_1 = 0.9St^2 [\sigma_\epsilon^2 T_{\epsilon\epsilon} - \rho_{\epsilon\zeta} \sigma_\epsilon \sigma_\zeta (T_{\epsilon\zeta} + T_{\zeta\epsilon}) + \sigma_\zeta^2 T_{\zeta\zeta}]. \quad (2.75)$$

We will see that both formulae are useful for interpreting the DNS and stochastic simulations.

2.3. Bidisperse RDF

We can extend the analysis to account for unlike particle pairs by incorporating the acceleration diffusivity, \mathcal{D}_\parallel^a , derived in §2.1.4. The resulting expression for the bidisperse RDF, $g_{12}(r)$, is

$$\frac{\partial g_{12}(r, t)}{\partial t} = \frac{1}{r^2} \frac{\partial [r^2 \text{Arg}_{12}(r, t)]}{\partial r} + \frac{1}{r^2} \frac{\partial}{\partial r} \left[r^2 (B_{nl} r^2 + \mathcal{D}_\parallel^a) \frac{\partial g_{12}(r, t)}{\partial r} \right]. \quad (2.76)$$

The steady-state solution of (2.76) under the assumptions and boundary condition used previously for the monodisperse case takes the form

$$g_{12}(r, \infty) = c_0 \left[\frac{\eta^2 + r_c^2}{r^2 + r_c^2} \right]^{c_1/2}, \quad (2.77)$$

where c_0 is an unspecified matching constant and c_1 is again expressed in two ways

$$c_1 = 3.61 \frac{St^{[s]}}{\Gamma_\eta^2} (\langle S^2 \rangle_p - \langle R^2 \rangle_p), \quad (2.78)$$

$$c_1 = 0.9St^{[s]} St^{[p]} [\sigma_\epsilon^2 T_{\epsilon\epsilon} - \rho_{\epsilon\zeta} \sigma_\epsilon \sigma_\zeta (T_{\epsilon\zeta} + T_{\zeta\epsilon}) + \sigma_\zeta^2 T_{\zeta\zeta}]. \quad (2.79)$$

The cross-over length r_c is defined as

$$\frac{r_c}{\eta} \equiv \left(\frac{\mathcal{D}_\parallel^a}{B_{nl}} \right)^{1/2} = \left(\frac{a_0 \Gamma_\eta \tau_a}{B_{nl}} \right)^{1/2} |St^{[p]} - St^{[s]}| \approx 5.0 |St^{[p]} - St^{[s]}|, \quad (2.80)$$

for $R_\lambda = 47.1$. Notice the competition between the two diffusive mechanisms. The shear diffusivity grows as r^2 , whereas the acceleration diffusivity is independent of r . Consequently, shear-driven diffusion is dominant for $\eta \gg r \gg r_c$ and a power-law pair probability similar to that found for a monodisperse suspension is recovered. Acceleration-driven diffusion dominates the shear mechanism for $r \ll r_c$, leading to an RDF that is independent of r in this limit. Equations (2.77)–(2.80) reproduce all of the qualitative trends observed in earlier DNS (Reade & Collins 2000b; Zhou *et al.* 2001).

3. Numerical simulations

The theory developed in §2 will be compared to the results from simulations of particles embedded in a turbulent flow field. The simulations differ from earlier ones (e.g. Sundaram & Collins 1997; Reade & Collins 2000b; Wang *et al.* 2000) in that

rather than following a population of particles in the laboratory frame of reference, we will follow a smaller number of primary particles and simulate the motion of surrounding satellite particles using a local linear flow approximation. In this way, the simulations directly test the theory under an identical set of assumptions. It is worth noting that the results from this simulation approach are in quantitative agreement with earlier ‘population’ studies. An important input to the simulations is the velocity gradient $\Gamma_{ij}^{[p]}(t)$ following a finite-inertia particle. The velocity gradient history will be generated from DNS (see § 3.2 for details) and from a stochastic model (see § 3.3 for details).

3.1. Satellite particle field

We simulate the relative motion of satellite particles in the frame of reference moving with a primary particle. The equations of motion for the satellite particles are given in (2.2), where $\Gamma_{ij}^{[p]}(t)$ and $a_i^{[p]}(t)$ will be supplied from DNS or from a stochastic model. For computational efficiency we typically simulate several hundred satellite particles surrounding each primary particle, and up to 10 000 primary particles to achieve statistical convergence. One complication with our simulation approach is that particle pairs will eventually diffuse to very large separation distances, making statistical convergence difficult. To alleviate this problem, we define a maximum spherical radius r_∞ beyond which we no longer simulate the satellite particles; that is, satellite particles with separation distances that exceed r_∞ are dropped from the simulation. This implies that, in the absence of a particle source, the satellite population will decrease with time. To replenish the satellite particles, we assume that particles can enter the spherical simulation domain from beyond r_∞ at a rate that is proportional to $|\mathbf{w} \cdot \mathbf{n}|$ for $\mathbf{w} \cdot \mathbf{n} < 0$ and zero otherwise, where \mathbf{n} is the unit outward normal on the spherical shell and the particle velocity $\hat{w}_i = \Gamma_{ij}^{[p]}(t)\hat{r}_j$ is that due to the local linear flow. At each time step, a number of attempts are made to produce a new satellite particle. For each attempt, a separation vector \hat{r} is generated with uniform probability on the spherical surface $\hat{r} = r_\infty$, a pair is then created with probability

$$P_{creation} = \frac{|\mathbf{w} \cdot \mathbf{n}|H(-\mathbf{w} \cdot \mathbf{n})}{|\mathbf{w} \cdot \mathbf{n}|_{max}}. \quad (3.1)$$

Estimating the maximum relative velocity as $|\mathbf{w} \cdot \mathbf{n}|_{max} = 2r_\infty \langle \Gamma_{11}^2 \rangle^{1/2} = 2r_\infty \Gamma_\eta / \sqrt{15}$ leads to a 2–3 % probability that $P_{creation}$ will be larger than one. In those cases, we generate one particle and use the remaining probability $P_{creation} - 1$ to determine whether a second particle should be generated. The number of trials for producing a satellite particle per iteration can be adjusted to control the average number of satellite particles per primary particle. (Note that the statistics of interest to this study are normalized such that they do not depend on the absolute number of satellite particles.) The introduction of a bounding surface does affect the RDF in the vicinity of the surface; however, we observe that the power-law behaviour for a monodisperse particle suspension is recovered for $r < 0.85r_\infty$ and so we only analyse the data within this inner shell.

Simulations with particles are run for approximately 20 Kolmogorov times to allow the satellite particles to equilibrate. The simulation volume $V \equiv 4\pi r_\infty^3/3$ is then divided into M spherical shells of volume V_1, \dots, V_M that sum to V . The RDF at an instant in time can be approximated by (Holtzer & Collins 2002)

$$g(\ell_i) = \frac{N_i/V_i}{Q/(4\pi r_\infty^2 |\mathbf{w} \cdot \mathbf{n}|_{max})}, \quad (3.2)$$

where ℓ_i is the mean radial position for volume V_i , N_i is the number of satellite particles contained within V_i , and Q is the number of trials for creating a particle per unit time. The normalization is chosen so that the RDF is approximately unity at $\ell_i = r_\infty$. Thus, the RDF can be thought of as the ratio of the number of satellite particles in a particular volume, N_i , to the expected number of satellite particles if the population were uniformly distributed. To improve the statistics, the RDF was averaged over time and, in the case of the DNS, over a multitude of primary particles located at independent positions throughout the DNS volume.

For the monodisperse system, we observe the expected power-law dependence for the RDF. To determine the coefficients of the power law, we perform a linear least-squares regression of

$$\ln g(\ell_i) = \ln c_0 + c_1 \ln \left(\frac{\eta}{\ell_i} \right), \quad (3.3)$$

to fit the parameters c_0 and c_1 . As already noted, c_0 has no physical meaning in this analysis, as there is no information on the transition away from the local linear flow approximation. We therefore restrict our attention to the behaviour of the regressed value for c_1 .

For the bidisperse cases, we performed a similar regression over the range $r_c \ll r_i < 0.85r_\infty$, where the power law approximation is expected to be valid, to determine c_0 and c_1 . To obtain a quantitative estimate of the cross-over radius, r_c , from the simulations, we assume the RDF takes the form predicted by theory (2.77) and solve for r_c , yielding

$$\frac{r_c^2}{\eta^2} = \frac{\left[\left(\frac{g_{12}(\ell_i)}{c_0} \right)^{2/c_1} \left(\frac{\ell_i}{\eta} \right)^2 - 1 \right]}{\left[1 - \left(\frac{g_{12}(\ell_i)}{c_0} \right)^{2/c_1} \right]}, \quad (3.4)$$

where $g_{12}(\ell_i)$ is the bidisperse RDF computed in a manner analogous to (3.2). We average the value of r_c obtained from each grid point satisfying $\ell_i < r_c$, using the previously regressed values of c_0 and c_1 . One important consideration with the bidisperse simulations is that the parameters must be carefully selected so that the transition from the power-law region to the constant asymptote occurs within the range of the simulation, i.e. $\ell_1 < r_c < 0.85r_\infty$. Theory enables us to estimate where this transition will occur so that appropriate values of the particle parameters can be selected.

3.2. Direct numerical simulations

The critical inputs to the particle simulations are the velocity gradient, $\Gamma_{ij}^{[p]}(t)$, and acceleration, $a_i^{[p]}(t)$, following a finite-inertia particle. Additionally, the theory requires the standard deviations and time correlations for several quantities. In this section, we describe direct numerical simulations (DNS) that are used to obtain these quantities. In principle, DNS introduces no modelling assumptions and therefore provides an *a priori* test of the theory.

DNS of isotropic turbulence in a periodic cube are performed under the assumption that the particle concentration field is sufficiently dilute that we can neglect the influence of the particles on the turbulence (i.e. ‘one-way’ coupling). The fluid flow is

Variable	Run 1	Run 2
u'	0.728	0.753
$\langle \epsilon \rangle$	0.152	0.160
ν	0.0126	0.0086
L	1.61	1.53
η	0.0597	0.0447
T_e	2.28	2.06
τ_η	0.289	0.234
R_λ	47.1	57.3
$k_{max}\eta$	1.92	2.15
σ_ϵ^2	0.02243	0.03083
σ_ζ^2	0.04323	0.06473
$\rho\epsilon\zeta$	0.430	0.472
$T_{\epsilon\epsilon}$	2.79	3.53
$T_{\zeta\zeta}$	5.51	5.88
$T_{\epsilon\zeta}$	6.05	7.63
$T_{\zeta\epsilon}$	3.83	4.94

TABLE 1. Relevant statistics from the direct numerical simulations. Run 1 was performed on a 64^3 lattice and Run 2 was performed on a 96^3 lattice. u' is the turbulent intensity, L is the integral length scale, η is the Kolmogorov length scale, $T_e \equiv L/u'$ is the large-eddy turnover time, $\tau_\eta \equiv \Gamma_\eta^{-1}$ is the Kolmogorov time scale and $k_{max}\eta$ is the product of the largest wavenumber with the Kolmogorov length scale, which is a measure of the resolution of the calculation (ideally greater than unity). All of the correlation times are normalized by the Kolmogorov time scale. The dimensional parameters are in arbitrary simulation units.

described by the continuity and Navier–Stokes equations

$$\frac{\partial u_i}{\partial x_i} = 0, \quad (3.5)$$

$$\frac{\partial u_i}{\partial t} + u_j \frac{\partial u_i}{\partial x_j} = -\frac{1}{\rho} \frac{\partial p}{\partial x_i} + \nu \frac{\partial^2 u_i}{\partial x_j \partial x_j} + F_i, \quad (3.6)$$

where ρ is the fluid density, p is the pressure and F_i is a stochastic forcing term, similar to the one described by Eswaran & Pope (1988), that maintains stationary turbulence. Details of the algorithm used to update the velocity can be found elsewhere (e.g. Sundaram & Collins 1997; Reade & Collins 2000a). Two simulations are performed at Taylor microscale Reynolds numbers $R_\lambda = 47.1$ and 57.3 (they will be referred to as Run 1 and Run 2); the relevant statistics are summarized in table 1. It should be noted that the resolution parameter, $k_{max}\eta$, is maintained at a relatively high value because the resolution at small scales is considered to be very important to describe properly the relative motion of particle pairs on sub-Kolmogorov length scales.

After the fluid reached a stationary state, point particles (representing the primary particles) are introduced at random positions throughout the periodic cell. The position and velocity of these point particles evolve according to (2.1). The particles are allowed to equilibrate with the flow for 4–6 large-eddy turnover times before statistics are taken. First, we evaluated Lagrangian statistics of the velocity gradient and acceleration that are required to complete the theory developed in §2 and the stochastic model discussed in §3.3 (see table 1 for a summary of the results). This includes the mean dissipation and enstrophy experienced along the finite-Stokes-number particle trajectory. Finally, the time-dependent velocity gradient and

acceleration in a reference frame following 10 000 finite-inertia particles is evaluated for the purpose of simulating the motion of satellite particles, as discussed above.

3.3. Stochastic simulations

In addition to the DNS, we developed a stochastic model for the velocity gradient, $\Gamma_{ij}^{[p]}(t)$, and acceleration, $a_i^{[p]}(t)$. The model is similar to those proposed by Girimaji & Pope (1990) and Brunk *et al.* (1998). However, one important limitation of these earlier models is that they do not capture the long-time correlations of dissipation and enstrophy, which play a crucial role in the proposed theory. Girimaji & Pope's model captures the long-time correlation of dissipation, but does not consider the enstrophy. Brunk *et al.* (1998) do not consider either of these statistics.

We begin by describing the model for the time variation of the dissipation and enstrophy. Earlier experimental evidence supports the assumption of a log normal distribution for both quantities. Consistent with this observation, we assume that the values of $\chi \equiv \ln \epsilon / \langle \epsilon \rangle$ and $\beta \equiv \ln \zeta / \langle \zeta \rangle$ at any two times t and $t + \tau$ have a joint normal distribution. This suggests that we can express the time evolution of the vector

$$\mathbf{X}(t) \equiv \begin{pmatrix} \chi(t) - \langle \chi \rangle \\ \beta(t) - \langle \beta \rangle \end{pmatrix}, \quad (3.7)$$

as an Ornstein–Uhlenbeck process (Gardiner 1985)

$$d\mathbf{X} = -\mathbf{A} \cdot \mathbf{X} dt + \mathbf{B} \cdot d\mathbf{W}(t), \quad (3.8)$$

where $d\mathbf{W}(t)$ is a vector-valued Wiener process satisfying the property

$$\langle d\mathbf{W}(t) \cdot d\mathbf{W}^T(s) \rangle = \delta(t - s) dt ds \mathbf{I}, \quad (3.9)$$

and \mathbf{I} is the identity tensor. The drift and diffusion matrices, \mathbf{A} and \mathbf{B} , are chosen to reproduce the variances, auto- and cross-correlation decay times for $\epsilon(t)$ and $\zeta(t)$ found in the DNS (see table 1). Details of the analysis used to obtain these coefficients and the resulting values that are obtained can be found in Appendix A.

To complete the model, we must relate the local rate of strain and rate of rotation tensors, S_{ik} and R_{ik} , to the fluctuating values of $\epsilon(t)$ and $\zeta(t)$. We define the rate of strain and rate of rotation tensors as follows

$$S_{ik} = P_{ik}(t) \sqrt{\frac{\epsilon(t)}{2\langle \epsilon \rangle}}, \quad (3.10a)$$

$$R_{ik} = Q_{ik}(t) \sqrt{\frac{\zeta(t)}{2\langle \zeta \rangle}}, \quad (3.10b)$$

where $P_{ik}(t)$ and $Q_{ik}(t)$ are joint normal random variables. These variables are produced by summing a series of sinusoidal functions of time with random coefficients and frequencies. The approach is similar to that developed by Kraichnan (1970) and is described in detail in Appendix B. Note that the coefficients and frequencies are chosen to satisfy the requirements of continuity and symmetry and to reproduce the temporal autocorrelations for the components of the strain and rotation tensors observed in DNS. Our model does not capture the exponential tails in the PDF of these quantities that are typically attributed to internal intermittency (Pope 2000). However it is believed that, as drift and diffusion of particle pairs are related to low-order moments of the velocity-gradient tensor, they are relatively insensitive to the tails of the distribution.

The model, up to this point, describes the velocity gradient along a fluid particle trajectory. In order to account for the bias in the sampling of strain and rotation by a finite-inertia particle, we must introduce the values of dissipation and enstrophy averaged along particle trajectories, $\langle \epsilon \rangle_p$ and $\langle \zeta \rangle_p$. To approximate this effect, we modify (3.10) as follows

$$S_{ik} = P_{ik}(t) \sqrt{\frac{\epsilon(t)}{2\langle \epsilon \rangle}} \sqrt{\frac{\langle \epsilon \rangle_p}{\langle \epsilon \rangle}}, \quad (3.11a)$$

$$R_{ik} = Q_{ik}(t) \sqrt{\frac{\zeta(t)}{2\langle \epsilon \rangle}} \sqrt{\frac{\langle \zeta \rangle_p}{\langle \epsilon \rangle}}. \quad (3.11b)$$

This approximation omits any changes to the correlation times of the rate of strain, rate of rotation, enstrophy and dissipation with St . These changes are likely to be small in the limit $St \ll 1$. In contrast, the $O(St)$ changes to $\langle \epsilon \rangle_p$ and $\langle \zeta \rangle_p$ are accounted for because they are essential to capture the leading-order drift term (see, for example, (2.15) and (2.16)).

3.4. Stochastic simulation of acceleration

To predict the radial distribution function of unlike particles (particles with different response times), we require a model for the fluid acceleration moving in a reference frame following the primary particle. To leading order, we can treat the particle trajectory as if it were a fluid trajectory. Sawford (1991) proposed a model for the acceleration of fluid particles in isotropic turbulence. The parameters in the model were determined by matching the resulting velocity autocorrelation function to the Kolmogorov similarity forms in the inertial and viscous subranges. The result is

$$d\mathbf{a} = -[\mathcal{C}\mathbf{a}(t) + \mathcal{E}\mathbf{u}(t)]dt + \mathcal{G}d\mathbf{W}(t), \quad (3.12)$$

where $\mathbf{u}(t)$ is the fluid velocity in the Lagrangian frame of reference, $\mathbf{a}(t) \equiv d\mathbf{u}/dt$ is the fluid acceleration and $d\mathbf{W}(t)$ is a vector-valued Wiener process subject to (3.9). According to Pope (2002), the coefficients \mathcal{C} , \mathcal{E} and \mathcal{G} are given by

$$\mathcal{C} = \frac{T_L}{\tau \tau_a}, \quad (3.13a)$$

$$\mathcal{E} = \frac{1}{\tau \tau_a}, \quad (3.13b)$$

$$\mathcal{G}^2 = \frac{2a_0 T_L \eta^2 \Gamma_\eta^4}{\tau \tau_a}, \quad (3.13c)$$

where T_L is the Lagrangian integral time scale and τ is the large-eddy turnover time defined as the ratio of the turbulent kinetic energy to the dissipation rate. From the definition of the turbulence time scale and classical scaling arguments, we can deduce the following

$$\tau \Gamma_\eta = \left(\frac{3}{20} \right)^{1/2} R_\lambda. \quad (3.14)$$

4. Results and discussion

In this section, we discuss the theoretical predictions derived in §2 and compare those predictions with DNS and stochastic simulations discussed in §3. Before

	$R_\lambda = 47.1$		$R_\lambda = 57.3$	
	Theory	DNS	Theory	DNS
$\langle \Delta S^2 \rangle$	0.122	0.119	0.045	0.063
$\langle \Delta R^2 \rangle$	-1.70	-1.72	-2.13	-2.15

TABLE 2. Table of normalized slopes $\langle \Delta S^2 \rangle$ and $\langle \Delta R^2 \rangle$ from theory and DNS.

discussing the results for the RDF for monodisperse and bidisperse particles given in §4.3 and §4.4, respectively, we will test two important steps in the theoretical development: (i) the prediction of the preference of primary particles to sample strain over rotational flows in §4.1; and (ii) the theoretical prediction for the non-local diffusion flux discussed in §4.2.

4.1. Dissipation and enstrophy experienced by particles

Recall that, whereas the average of $\langle S^2 \rangle$ and $\langle R^2 \rangle$ along a fluid trajectory is equal to $\Gamma_\eta^2/2$, the average of the same quantities along particle trajectories, i.e. $\langle S^2 \rangle_p$ and $\langle R^2 \rangle_p$, will deviate from this value. The degree of deviation increases linearly with St for $St \ll 1$, making it convenient to define slope parameters as follows

$$\langle \Delta S^2 \rangle \equiv \frac{\langle S^2 \rangle_p - \langle S^2 \rangle}{St(\Gamma_\eta^2/2)}, \quad (4.1a)$$

$$\langle \Delta R^2 \rangle \equiv \frac{\langle R^2 \rangle_p - \langle R^2 \rangle}{St(\Gamma_\eta^2/2)}. \quad (4.1b)$$

From (2.39) and (2.39), we can write the theoretical predictions for these quantities

$$\langle \Delta S^2 \rangle = \frac{1}{2} [\sigma_\epsilon^2 T_{\epsilon\epsilon} - \rho_{\epsilon\zeta} \sigma_\epsilon \sigma_\zeta T_{\epsilon\zeta}], \quad (4.2a)$$

$$\langle \Delta R^2 \rangle = \frac{1}{2} [\rho_{\epsilon\zeta} \sigma_\epsilon \sigma_\zeta T_{\zeta\epsilon} - \sigma_\zeta^2 T_{\zeta\zeta}]. \quad (4.2b)$$

A comparison of (4.2) with values obtained from DNS measurements along finite-inertia particle tracks is shown in table 2. The theoretical predictions are in very good agreement with the DNS and appear to capture the effect of the Reynolds number. Similar agreement can be seen in figure 1, which shows the raw data. Notice that the linear regime for $\langle S^2 \rangle_p$ extends to $St = 0.2$, whereas the linear regime for $\langle R^2 \rangle_p$ is valid only over the range $0 < St < 0.05$. The linear theory does not take into consideration second-order effects due to the depletion of particles in regions of high rotation. Apparently this becomes significant for $St > 0.05$, where the variation of $\langle R^2 \rangle_p$ with St is decreasing. This change in the slope of $\langle R^2 \rangle_p$ is not surprising since we expect the curve will pass through a minimum before returning to the fluid particle value of $\Gamma_\eta^2/2$ in the limit $St \rightarrow \infty$. This is because the motion of highly inertial particles is insensitive to the flow.

A more subtle question concerns the dependence of $\langle \Delta S^2 \rangle$ and $\langle \Delta R^2 \rangle$ on the Reynolds number. According to (4.2), $\langle \Delta S^2 \rangle$ and $\langle \Delta R^2 \rangle$ are linearly related to the correlation times for dissipation and/or enstrophy. As dissipation and enstrophy vary over integral time scales, these correlation times, non-dimensionalized by Γ_η , would appear to make $\langle \Delta S^2 \rangle$ and $\langle \Delta R^2 \rangle$ proportional to R_λ . As seen in table 2, this behaviour is observed for $\langle \Delta R^2 \rangle$; however, the opposite trend is found with $\langle \Delta S^2 \rangle$. That is, $\langle \Delta S^2 \rangle$ decreases with increasing Reynolds number. To understand the difference in these two statistics, it is useful to recall that $\langle \Delta S^2 \rangle$ involves the difference

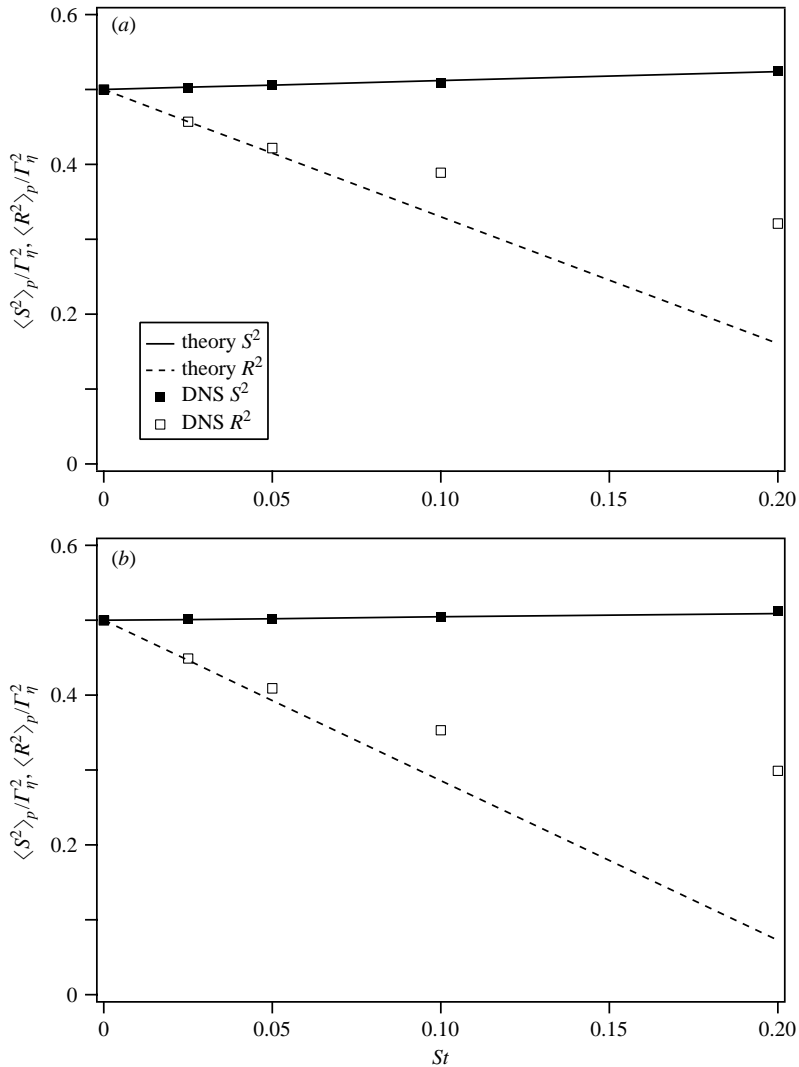


FIGURE 1. Plots of $\langle S^2 \rangle_p / \Gamma_\eta^2$ and $\langle R^2 \rangle_p / \Gamma_\eta^2$ as a function of St for (a) $R_\lambda = 47.1$ and (b) $R_\lambda = 57.3$. Solid and dashed lines denote the theoretical predictions for $\langle \Delta S^2 \rangle_p$ and $\langle \Delta R^2 \rangle_p$, respectively. The filled and open squares are the respective DNS values.

between the dissipation autocorrelation time scale and the enstrophy-dissipation cross-correlation time scale, whereas $\langle \Delta R^2 \rangle$ involves the difference between the enstrophy autocorrelation time scale and the enstrophy-dissipation cross-correlation time scale. In $\langle \Delta R^2 \rangle$, the enstrophy autocorrelation time scale is dominant and the cross-correlation has a lesser influence. This can be physically attributed to the impact of the vortex tubes, which are more highly intermittent than strain and persist for longer periods of time (Batchelor 1967). With increasing R_λ , the strength and persistence of the vortex tubes increases, causing the correlation $\langle \Delta R^2 \rangle$ to steadily decrease. In contrast, $\langle \Delta S^2 \rangle$ is determined by the difference of quantities that are nearly in balance, and hence the trend with R_λ depends on relative changes of the two time scales. The net result is a decreasing function of R_λ , at least over the range

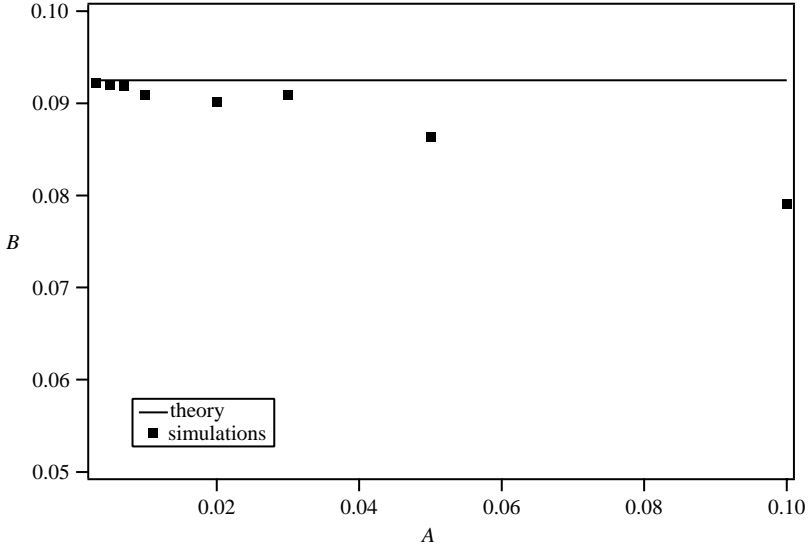


FIGURE 2. The coefficient B for non-local pair diffusion determined from simulations of (4.3) as a function of the drift parameter A . The solid line denotes the theoretical prediction, (2.60), and the filled squares denote the simulation data.

we explored in the DNS. The impact of these trends has important implications for collision kernels that are discussed at greater length in Collins & Keswani (2004).

4.2. Non-local diffusion flux

In §2.1.3, we derived the pair diffusivity resulting from shear based on a simplified model of the velocity gradient tensor. To test this model, we perform a series of simulations of fluid particles with an imposed (artificial) inward drift velocity. The governing equation for the satellite particles takes the form

$$\frac{d\hat{r}_i}{dt} = -A\Gamma_\eta\hat{r}_i + \Gamma_{ij}(t)\hat{r}_j. \quad (4.3)$$

We control the strength of the drift by varying the parameter A above. Simulations of (4.3) produce a power law RDF in which $c_1 = A/B$. We can determine B from these simulations by fitting c_1 for a given A and computing $B = A/c_1$. This is therefore an independent test of the diffusion model. Figure 2 shows a plot of B for various values of A . The flux is in very good agreement with the theory for $A \leq 0.03$, corresponding to $c_1 \leq 0.3$. It will be seen in the next section that the power-law exponents resulting from inertial drift fall within the range of validity of the approximation for the pair diffusion flux.

4.3. RDF for monodisperse particles

The power-law exponent, c_1 , predicted by the theory can be obtained by substituting the variances and time correlations from the DNS given in table 1 into (2.75), yielding $c_1 = 6.56St^2$ for $R_\lambda = 47.1$. The power-law exponent obtained from a fit of the simulation data (both DNS and stochastic velocity gradients) is compared to this prediction in figure 3. As you can see, there is excellent agreement between the theory (solid line) and both simulations (solid and open squares) for $St < 0.1$; however, at larger Stokes numbers, the theory is over-predicting the coefficient. This error can be traced to the assumption of a linear dependence of $\langle S^2 \rangle_p$ and $\langle R^2 \rangle_p$ on Stokes

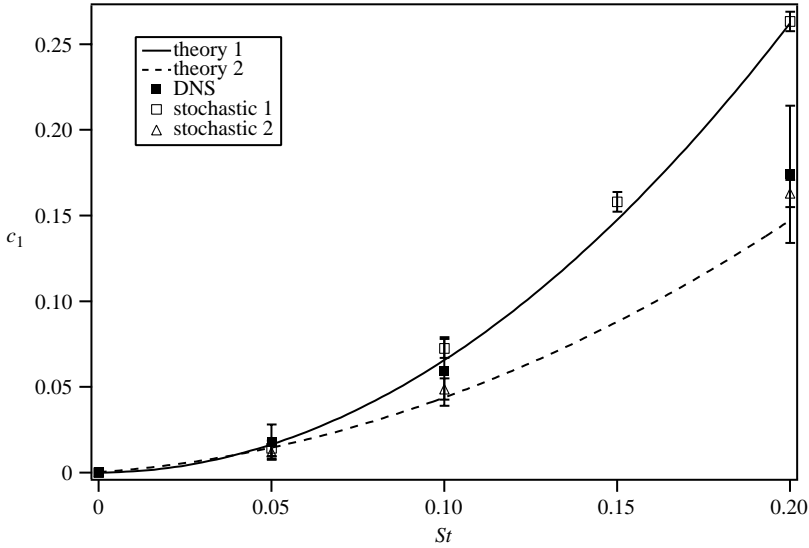


FIGURE 3. Values of c_1 as a function of particle Stokes number for a monodisperse system of particles at $R_\lambda = 47.1$. The solid line is the theoretical prediction using (2.75), which for this Reynolds number yields $c_1 = 6.558St^2$, and the dashed line is the theoretical prediction using (2.74) and DNS values of $\langle S^2 \rangle_p$ and $\langle R^2 \rangle_p$. ■, DNS results (error bars denote 90 % confidence intervals); □, stochastic simulation using the linear theory estimate of $\langle S^2 \rangle_p$ and $\langle R^2 \rangle_p$; △, the same simulation but with DNS values of $\langle S^2 \rangle_p$ and $\langle R^2 \rangle_p$.

number. As observed in figure 1, the dependence of $\langle R^2 \rangle_p$ deviates from the linear approximation for $St > 0.1$. To confirm this, we show the values of c_1 determined from (2.74) using values of $\langle S^2 \rangle_p$ and $\langle R^2 \rangle_p$ obtained directly from DNS (dashed line). The agreement is within the error tolerance over the entire range of Stokes numbers. Thus, the framework of the theory is valid over a range of Stokes numbers that exceeds the linear regime for $\langle S^2 \rangle_p$ and $\langle R^2 \rangle_p$, if the means for predicting these quantities becomes available. The extension of the theory for $\langle S^2 \rangle_p$ and $\langle R^2 \rangle_p$ beyond the linear regime will be the topic of a future paper.

It should be noted that the quadratic dependence of c_1 on Stokes number (for $St < 0.1$) was previously predicted by Balkovsky *et al.* (2001) and again by Zaichik & Alipchenkov (2003) using different approaches. However, the prefactors predicted by these theories, and its dependence on the variances and time correlations of the dissipation and enstrophy, are not in agreement with our prediction (6.56 for $R_\lambda = 47.1$). Consequently, their predictions are not in quantitative agreement with the DNS results presented here.

4.4. RDF for bidisperse particles

A series of runs were done with a primary particle Stokes number of $St^{[p]} = 0.2$ and satellite Stokes numbers of $St^{[s]} = 0.195, 0.19$ and 0.175 . Figure 4 shows the theoretical prediction for the RDF for $St^{[s]} = 0.175, 0.19$ and 0.2 (corresponding to the monodisperse result). The monodisperse result yields the familiar power law, whereas the bidisperse cases are initially power law for large separations, but transition to a constant value for $r < r_c$, where the theoretical prediction for r_c is $r_c/\eta = 5|St^{[p]} - St^{[s]}|$. Stochastic simulations, in which $\langle S^2 \rangle_p$ and $\langle R^2 \rangle_p$ are specified by (2.39), are performed to test the theory. We use these values (rather than DNS values) to eliminate the error

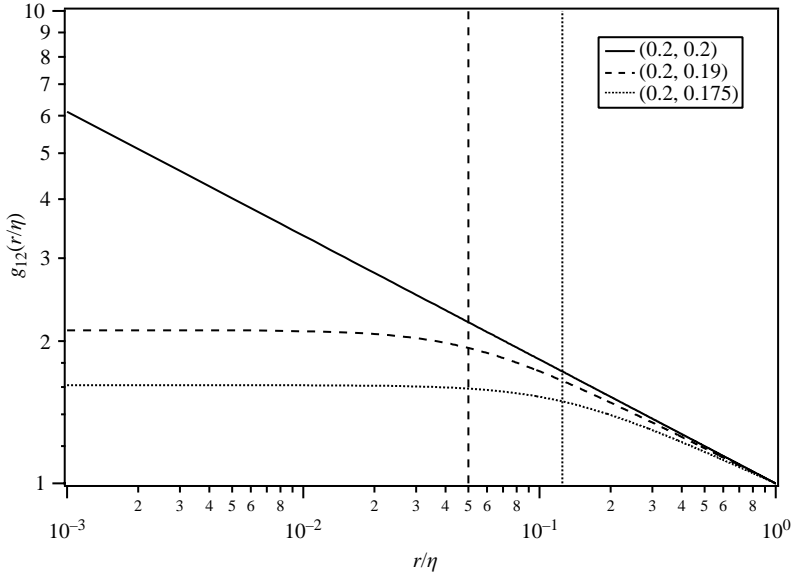


FIGURE 4. Radial distribution function for bidisperse mixtures with a primary particle Stokes number of $St^{[p]}=0.2$ and satellite particle Stokes numbers of $St^{[s]}=0.2$ (solid line, corresponding to the monodisperse case), 0.19 (dashed line) and 0.175 (dotted line) predicted by theory with the cross-over length given by $\hat{r}_c/\eta = 5|St^{[p]} - St^{[s]}|$ (the result for $R_\lambda = 47.1$). Vertical lines indicate \hat{r}_c/η for $St^{[s]}=0.19$ (dashed line) and 0.175 (dotted line).

Stokes number		c_1		r_c/η		
$St^{[p]}$	$St^{[s]}$	Theory	Stochastic simulations	Theory	DNS	Stochastic simulations
0.175	0.175	0.201	0.209 ± 0.006			
0.19	0.19	0.237	0.241 ± 0.006			
0.195	0.195	0.249	0.252 ± 0.006			
0.2	0.2	0.262	0.263 ± 0.006			
0.2	0.195	0.256	0.258 ± 0.005	0.025	0.033 ± 0.005	0.028 ± 0.005
0.2	0.19	0.249	0.255 ± 0.005	0.050	0.054 ± 0.005	0.047 ± 0.006
0.2	0.175	0.230	0.236 ± 0.005	0.125	0.133 ± 0.005	0.126 ± 0.008

TABLE 3. Power-law exponents, c_1 and cross-over lengths, r_c/η for the bidisperse and relevant monodisperse cases corresponding to $R_\lambda=47.1$. Errors in the simulations denote 90% confidence intervals.

associated with the assumption of a linear dependence of $\langle R^2 \rangle_p$ on Stokes number (see discussion in §4.3). Alternatively, we can simulate smaller values of the Stokes number to ensure we are within the linear regime; unfortunately, we cannot achieve sufficient statistical convergence at these smaller values of Stokes number to determine r_c/η . Hence we use larger values of Stokes number and base the comparisons of c_1 on the stochastic simulations alone. Table 3 shows the comparison. In all cases, the predictions are within the 90% confidence interval of the simulation result.

Next, we consider the cross-over radius, r_c/η . The values predicted by the theory are compared to DNS and the stochastic simulations in table 3. In general, the agreement with the DNS is very good, although not quite as good as the comparison with the

stochastic simulations. This is due in part to the differences in the c_1 values in the DNS that is not corrected for. Indeed given this discrepancy, the agreement in r_c/η is remarkably good.

5. Implications for coagulating aerosols

The theoretical predictions from this study are in quantitative agreement with DNS and stochastic simulations, giving us confidence in considering the implications the theory has for predicting the collision kernel of a coagulating or coalescing aerosol. The theory is limited to the regime $St \ll 1$, and so we will restrict our attention accordingly; nevertheless, there are a number of systems that fall into this regime that can be analysed by this theory. For example, the open questions concerning the evolution of stratocumulus clouds and the formation of rain fall into this category (Shaw 2003). The relative significance of turbulence-driven coalescence and clustering versus coalescence due to gravitational settling (neglected in this study) is still openly debated. Another example is aerosol processing of powders (Pratsinis, Zhu & Vemury 1996), wherein turbulence in the device may play a critical role in determining the product particle size distribution.

As we are concerned with the regime of small Stokes numbers, the starting point is the famous result by Saffman & Turner (1956), who predicted the collision kernel for a monodisperse system of particles, in the limit $St \rightarrow 0$ to be

$$\tilde{K} = 1.1\Gamma_\eta d^3, \quad (5.1)$$

where d is the particle diameter and the coefficient 1.1 is the value corrected by Brunk *et al.* (1998) for the lack of persistence in the velocity gradient.† Sundaram & Collins (1997) showed that the collision kernel corrected for clustering, designated K , is given by

$$K = \tilde{K} g(d). \quad (5.2)$$

For a monodisperse population of particles satisfying $St \ll 1$ and $d \ll \eta$, we can write this approximately as

$$K = 1.1\Gamma_\eta d^3 c_0 \left(\frac{\eta}{d}\right)^{c_1}. \quad (5.3)$$

Although $c_1 \propto St^2$ and is therefore small, the enhancement can still be significant for large η/d .

Next we consider the collision kernel for unlike particles. Recall that the bidisperse RDF ceases to follow a power law scaling with r and approaches a constant value for $r < r_c$. The simplest postulate for the bidisperse collision kernel is to multiply the monodisperse kernel by the bidisperse RDF evaluated at contact. This postulate would lead to a lower collision kernel for unlike particles. However, turbulent accelerations acting on unlike particles will also increase their relative velocity, potentially offsetting the decrease in the RDF factor. We can estimate the net change in the collision kernel due to both effects. To facilitate this, it is useful to define the bidisperse collision kernel as

$$K_{12} = \gamma 1.1\Gamma_\eta d_{12}^3 c_0 \left(\frac{\eta}{d_{12}}\right)^{c_1}, \quad (5.4)$$

† Originally Saffman & Turner (1956) predicted the value 1.3 under the assumption that the correlation time for strain and rotation is infinite. Brunk *et al.* (1998) corrected this value by using more realistic correlation times determined from DNS.

	$St^{[s]}$	$St^{[p]}$	γ	γ_{S-T}
Polydisperse	0.175	0.2	2.54	4.47
	0.19	0.2	2.16	2.45
	0.195	0.2	1.62	1.93
Monodisperse	0.2	0.2	1.19	—

TABLE 4. The coagulation kernel ratio γ defined in (5.4), from stochastic simulations corresponding to $R_\lambda = 47.1$. The value γ_{S-T} is obtained from (5.6).

where $d_{12} \equiv (d_1 + d_2)/2$ is the mean collision diameter and γ is the correction factor we introduce to account for both the reduction in the RDF and the enhancement in the relative velocity due to acceleration-driven relative motions. The value of γ (relative to unity) determines which effect is dominant. If we assume $d_{12} < r_c$, we can approximate the collision kernel as $\mathcal{D}^{[a]} d_{12} g_{12}(d_{12})$, and obtain a scaling relationship for γ

$$\gamma \propto \left(\frac{r_c}{d_{12}} \right)^{2-c_1}, \quad (5.5)$$

which suggests that the bidisperse collision kernel is enhanced by acceleration-driven motions when $d_{12} < r_c$. Here, we have assumed that the dominant diffusivity is due to acceleration, which is valid when $d_{12} < r_c$; under the opposite circumstance, $d_{12} > r_c$, the collision kernel is dominated by shear (rather than acceleration) and $\gamma \approx 1$.

To obtain more quantitative results, we have performed stochastic simulations and measured the collision kernel and enhancement factor, γ . The conditions we simulate correspond to $St^{[p]} = 0.2$ and $St^{[s]} = 0.175, 0.19$ and 0.195 . The ratio η/d_{12} is taken to be 50, which is a reasonable value for turbulent coagulation. Results of the simulations are reported in table 4. Notice that in all three cases $\gamma > 1$, confirming the earlier scaling given in (5.5). In addition to the simulations, we show the prediction by Saffman & Turner (1956), multiplied by the enhancement factor for clustering (RDF at contact). Writing their expression in terms of the variables we have defined yields

$$\gamma_{S-T} = \left(\frac{8}{8.62} \right) (2\pi)^{1/2} \left[(St^{[p]} - St^{[s]})^2 a_0 \left(\frac{2\eta}{d_{12}} \right)^2 + \frac{4}{9} \right]^{1/2} \left(\frac{d_{12}}{r_c} \right)^{c_1}. \quad (5.6)$$

This relationship gives qualitatively reasonable results (see table 4), but overpredicts the enhancement factor for the lower values of $St^{[s]}$. The overprediction is probably due to their assumption that the acceleration remains correlated over the time scale of the particle encounter. In practice, we find that the persistence length for the relative motion of two particles is comparable with the mean particle diameter, d_{12} .

6. Conclusions

We have developed a theory to describe the clustering of aerosol particles in isotropic turbulence in the limit $St \ll 1$. Motivated by the observation that much of the growth of the RDF occurs at particle separations smaller than the Kolmogorov length scale, η , the theory is based on a local linear flow approximation for the fluid velocity. The theory has been validated by extensive comparisons with DNS and stochastic simulations.

Sub-Kolmogorov clustering occurs because of particle inertia and the fact that finite-inertia particles sample more strain than rotation. Our analysis of the equations

for the velocity and the probability density function for particle pairs shows that the bias in sampling strain over rotation is proportional to the Stokes number. Moreover, our prediction of $\langle S^2 \rangle_p$ and $\langle R^2 \rangle_p$ are in quantitative agreement with DNS for $St < 0.05$ and $R_\lambda = 47.1$ and 57.3 .

The theory for the RDF involves predictions of the drift and diffusion fluxes for the particle pairs. Drift terms are obtained by a perturbation expansion in the Stokes number. The diffusion flux is shown to be non-local, and hence a new analysis has been developed to obtain a closed expression for this quantity. The resulting expression has an integral involving the RDF (rather than the gradient of the RDF, as would be obtained for local diffusion); however, this result can be simplified under the assumption of a power-law behaviour for the RDF at small separations. The resulting expression for the shear diffusivity has the same form as was found from the local analysis, but with a coefficient reduced by 40%. Comparisons with stochastic simulations confirm the result. Diffusion for bidisperse particles (i.e. particles with different Stokes numbers) is enhanced by an acceleration-driven flux. A closed-form expression for this diffusivity is derived based on the correlation time for fluid accelerations. One consequence of this second diffusivity, which is independent of particle separation, is that the RDF for unlike particles deviates from the power-law at separations below a cut-off separation, r_c , and approaches a constant. The theory is able to predict the power-law for monodisperse and bidisperse particles as well as the cut-off separation for the latter in quantitative agreement with both DNS and stochastic simulations.

Finally, we explored some of the consequences of clustering on the collision kernel for particles in the limit $St \ll 1$. The enhancement to the collision kernel is proportional to $(\eta/d)^{c_1}$. Although c_1 is proportional to St^2 (for $St < 0.05$), the enhancement can still be significant for circumstances where $\eta/d \gg 1$. The collision kernel for unlike particles is attenuated owing to a reduction in clustering, but augmented by the increased relative velocity due to accelerations. The net effect is shown to be an enhancement for the circumstance $d_{12} < r_c$. This may help explain the rather dramatic effects of clustering on the particle size distribution of coagulating aerosols observed in earlier DNS performed by Reade & Collins (2000*b*).

This work was supported by NASA grants: NAG3-2349 (JC and DLK) and NAG3-2470 (SLR, AA and LRC) and by the National Science Foundation grant PHY-0216406 (LRC).

Appendix A. Stochastic differential equation for dissipation and enstrophy

The stochastic model introduced in §3.3 (see (3.8) and related discussion) requires relationships for the drift and diffusion matrices, \mathbf{A} and \mathbf{B} . This appendix discusses how these matrices are obtained.

Recall that we define $\chi(t) \equiv \ln[\epsilon(t)/\langle \epsilon \rangle]$ and $\beta(t) \equiv \ln[\zeta(t)/\langle \zeta \rangle]$ as joint normal variables. We define $\mathbf{X}(t)$ as

$$\mathbf{X}(t) \equiv \begin{pmatrix} \chi(t) - \langle \chi \rangle \\ \beta(t) - \langle \beta \rangle \end{pmatrix}. \quad (\text{A } 1)$$

The time evolution of $\mathbf{X}(t)$ is modelled as a vector-valued Ornstein–Uhlenbeck process

$$d\mathbf{X} = -\mathbf{A} \cdot \mathbf{X} dt + \mathbf{B} \cdot d\mathbf{W}(t), \quad (\text{A } 2)$$

where **A** and **B** define the correlations and time constants for $\chi(t)$ and $\beta(t)$. To determine these matrices, we must first relate the intrinsic variables of the Ornstein–Uhlenbeck process (i.e. σ_χ , σ_β , $\rho_{\chi\beta}$, $T_{\chi\chi}$, $T_{\chi\beta}$, $T_{\beta\chi}$ and $T_{\beta\beta}$) to the known properties of $\epsilon(t)$ and $\zeta(t)$ (i.e. $\langle\epsilon\rangle$, σ_ϵ , σ_ζ , $\rho_{\epsilon\zeta}$, $T_{\epsilon\epsilon}$, $T_{\epsilon\zeta}$, $T_{\zeta\epsilon}$ and $T_{\zeta\zeta}$).

A.1. *Single-time statistics*

We begin with the single-time correlations and cross-correlations of $\chi(t)$ and $\beta(t)$. Under the assumption that they are joint normally distributed we have (Pope 2000)

$$\langle\epsilon^m(t)\zeta^n(t)\rangle = \langle\epsilon\rangle^{(m+n)}\exp\left[\frac{1}{2}m(m-1)\sigma_\chi^2 + mn\rho_{\chi\beta}\sigma_\chi\sigma_\beta + \frac{1}{2}n(n-1)\sigma_\beta^2\right]. \tag{A 3}$$

Setting $m = 2$ and $n = 0$ yields (after rearranging)

$$\sigma_\chi^2 = \ln(1 + \sigma_\epsilon^2). \tag{A 4}$$

Equivalently, setting $m = 0$ and $n = 2$ yields

$$\sigma_\beta^2 = \ln(1 + \sigma_\zeta^2). \tag{A 5}$$

Finally selecting $m = 1$ and $n = 1$ yields

$$\rho_{\chi\beta} = \frac{\ln(1 + \rho_{\epsilon\zeta}\sigma_\epsilon\sigma_\zeta)}{\sigma_\chi\sigma_\beta}. \tag{A 6}$$

These relationships allow us to determine σ_χ , σ_β and $\rho_{\chi\beta}$ in terms of σ_ϵ , σ_ζ and $\rho_{\epsilon\zeta}$. Under the normalization we are using we can further state

$$\langle\chi\rangle = -\frac{1}{2}\sigma_\chi^2 = -\frac{\ln(1 + \sigma_\epsilon^2)}{2}, \tag{A 7}$$

$$\langle\beta\rangle = -\frac{1}{2}\sigma_\beta^2 = -\frac{\ln(1 + \sigma_\zeta^2)}{2}. \tag{A 8}$$

A.2. *Time correlations*

Next we consider two-time statistics to derive the correlation times of the model. We define the general time correlation function as

$$\mathcal{F}_{\chi\beta}(\tau) \equiv \frac{\langle(\chi(t) - \langle\chi\rangle)(\beta(t + \tau) - \langle\beta\rangle)\rangle}{\rho_{\chi\beta}\sigma_\chi\sigma_\beta}. \tag{A 9}$$

For an Ornstein–Uhlenbeck process,

$$\mathcal{F}_{\chi\beta}(\tau) = \exp(-\tau/T_{\chi\beta}), \tag{A 10}$$

where $T_{\chi\beta}$ is the integral time scale. Equivalent expressions for the related correlation functions $\mathcal{F}_{\chi\chi}(\tau)$, $\mathcal{F}_{\beta\chi}(\tau)$ and $\mathcal{F}_{\beta\beta}(\tau)$ are defined by analogy.

We can construct correlation functions for $\epsilon(t)$ and $\zeta(t)$ from these definitions. For example,

$$\begin{aligned} \mathcal{F}_{\epsilon\epsilon}(\tau) &= \frac{\langle\epsilon\rangle^2\langle(\exp[\chi(t)] - 1)(\exp[\chi(t + \tau)] - 1)\rangle}{\sigma_\epsilon^2\langle\epsilon\rangle^2} \\ &= \frac{\langle\exp[\chi(t) + \chi(t + \tau)] - \langle\exp[\chi(t)]\rangle - \langle\exp[\chi(t + \tau)]\rangle + 1}{\sigma_\epsilon^2} \\ &= \frac{\langle\exp[\chi(t) + \chi(t + \tau)]\rangle - 1}{\sigma_\epsilon^2}. \end{aligned} \tag{A 11}$$

Variable	$R_\lambda = 47.1$	$R_\lambda = 57.3$
σ_χ	0.8229	0.8875
σ_β	1.0262	1.1213
$\rho_{\chi\beta}$	0.5402	0.6015
$T_{\chi\chi}$	3.33	4.34
$T_{\beta\beta}$	7.31	8.28
$T_{\chi\beta}$	6.78	8.93
$T_{\beta\chi}$	4.29	5.78

TABLE 5. Summary of intrinsic parameters for the stochastic model for $\chi(t)$ and $\beta(t)$, determined from (A 4)–(A 6) and (A 14)–(A 17). Note that the time correlations are all normalized by the Kolmogorov time.

Substituting (A 10) yields

$$\mathcal{F}_{\epsilon\epsilon}(\tau) = \frac{\exp[\sigma_\chi^2 \mathcal{F}_{\chi\chi}(\tau)] - 1}{\sigma_\epsilon^2} = \frac{\exp[\sigma_\chi^2 \exp(-\tau/T_{\chi\chi})] - 1}{\sigma_\epsilon^2}. \quad (\text{A } 12)$$

Notice that the correlation function $\mathcal{F}_{\epsilon\epsilon}(\tau)$ is not exponential. To relate the time correlation $T_{\epsilon\epsilon}$, defined as

$$T_{\epsilon\epsilon} \equiv \int_0^\infty \mathcal{F}_{\epsilon\epsilon}(\tau) d\tau, \quad (\text{A } 13)$$

to $T_{\chi\chi}$, we integrate (A 12) and obtain (after rearranging)

$$T_{\chi\chi} = \frac{\sigma_\epsilon^2 T_{\epsilon\epsilon}}{[\text{Ei}(\sigma_\chi^2) - \ln(\sigma_\chi^2) - \gamma_E]}, \quad (\text{A } 14)$$

where $\gamma_E = 0.57216$ is Euler's constant and $\text{Ei}(z)$ is the exponential integral function (Abramowitz & Stegun 1964). We can derive similar relationships for the other three time correlations

$$T_{\beta\beta} = \frac{\sigma_\zeta^2 T_{\zeta\zeta}}{[\text{Ei}(\sigma_\beta^2) - \ln(\sigma_\beta^2) - \gamma_E]}, \quad (\text{A } 15)$$

$$T_{\chi\beta} = \frac{\rho_{\epsilon\zeta} \sigma_\epsilon \sigma_\zeta T_{\epsilon\zeta}}{[\text{Ei}(\rho_{\chi\beta} \sigma_\chi \sigma_\beta) - \ln(\rho_{\chi\beta} \sigma_\chi \sigma_\beta) - \gamma_E]}, \quad (\text{A } 16)$$

$$T_{\beta\chi} = \frac{\rho_{\epsilon\zeta} \sigma_\epsilon \sigma_\zeta T_{\zeta\epsilon}}{[\text{Ei}(\rho_{\chi\beta} \sigma_\chi \sigma_\beta) - \ln(\rho_{\chi\beta} \sigma_\chi \sigma_\beta) - \gamma_E]}. \quad (\text{A } 17)$$

A summary of the results obtained from (A 4)–(A 6) and (A 14)–(A 17) is given in table 5.

A.3. Drift and diffusion matrices

Given the auto- and cross-correlations and all of the correlation times, it is possible to determine the drift matrix \mathbf{A} and diffusion matrix \mathbf{B} . The analysis used to determine these matrices can be found in Gardiner (1985, pp. 109–112). To begin, we define two additional matrices

$$\Sigma \equiv \begin{pmatrix} \sigma_\chi^2 & \rho_{\chi\beta} \sigma_\chi \sigma_\beta \\ \rho_{\chi\beta} \sigma_\chi \sigma_\beta & \sigma_\beta^2 \end{pmatrix}, \quad (\text{A } 18)$$

R_i	\mathbf{A}	\mathbf{B}
47.1	$\begin{bmatrix} 0.3364 & -0.0262 \\ 0.0227 & 0.1310 \end{bmatrix}$	$\begin{bmatrix} 0.6570 & 0.0 \\ 0.3074 & 0.4522 \end{bmatrix}$
57.3	$\begin{bmatrix} 0.2932 & -0.0398 \\ -0.0290 & 0.1304 \end{bmatrix}$	$\begin{bmatrix} 0.6433 & 0.0 \\ 0.2832 & 0.4654 \end{bmatrix}$

TABLE 6. Table of coefficients in the \mathbf{A} and \mathbf{B} matrices used in (3.8).

$$\mathbf{G} \equiv \begin{pmatrix} \sigma_\chi^2 T_{\chi\chi} & \rho_{\chi\beta} \sigma_\chi \sigma_\beta T_{\beta\chi} \\ \rho_{\chi\beta} \sigma_\chi \sigma_\beta T_{\chi\beta} & \sigma_\beta^2 T_{\beta\beta} \end{pmatrix}, \quad (\text{A } 19)$$

both of which are determined by the relationships given in (A 4)–(A 6) and (A 14)–(A 17). Following Gardiner, we have

$$\langle \mathbf{X}(t + \tau) \mathbf{X}^T(t) \rangle = \exp[-\mathbf{A}\tau] \cdot \boldsymbol{\Sigma}. \quad (\text{A } 20)$$

Integrating both sides with respect to τ from 0 to ∞ gives

$$\mathbf{G} = \mathbf{A}^{-1} \cdot \boldsymbol{\Sigma}. \quad (\text{A } 21)$$

Rearranging yields an expression for \mathbf{A}

$$\mathbf{A} = \boldsymbol{\Sigma} \cdot \mathbf{G}^{-1}, \quad (\text{A } 22)$$

Gardiner also showed that

$$\mathbf{B} \cdot \mathbf{B}^T = \mathbf{H}, \quad (\text{A } 23)$$

where

$$\mathbf{H} \equiv \mathbf{A} \cdot \boldsymbol{\Sigma} + \boldsymbol{\Sigma} \cdot \mathbf{A}^T. \quad (\text{A } 24)$$

To find a solution for \mathbf{B} , we note that since \mathbf{H} is a symmetric positive definite matrix (guaranteed by the form of (A 24)), we can apply a Cholesky decomposition and express \mathbf{B} as a lower-triangular matrix of the form

$$\mathbf{B} = \begin{pmatrix} b_{11} & 0 \\ b_{21} & b_{22} \end{pmatrix}. \quad (\text{A } 25)$$

The coefficients of the \mathbf{B} matrix are then obtained in sequence as shown below

$$b_{11} = \sqrt{h_{11}}, \quad (\text{A } 26)$$

$$b_{21} = h_{12}/b_{11}, \quad (\text{A } 27)$$

$$b_{22} = \sqrt{h_{22} - b_{21}^2}, \quad (\text{A } 28)$$

where

$$\mathbf{H} = \begin{pmatrix} h_{11} & h_{12} \\ h_{12} & h_{22} \end{pmatrix}. \quad (\text{A } 29)$$

The values of the drift and diffusion matrices used in this study are listed in table 6.

Appendix B. Normalized strain and rotation rate tensors, $P_{ik}(t)$ and $Q_{ik}(t)$

The velocity gradient model given in § 3.3 requires that the random unit tensors $P_{ik}(t)$ and $Q_{ik}(t)$ be specified. The approach we use is similar to the one taken by

Brunk *et al.* (1998). A random Fourier series is written as

$$P_{ik}(t) = \sum_{n=1}^N [\widehat{P}_{ik}^n \exp(i\pi\omega_p^n t)], \quad (\text{B } 1)$$

$$Q_{ik}(t) = \sum_{n=1}^N [\widehat{Q}_{ik}^n \exp(i\pi\omega_q^n t)], \quad (\text{B } 2)$$

where N is the number of terms in the series (usually between 200 and 1000). The coefficients, \widehat{P}_{ik}^n , \widehat{Q}_{ik}^n , ω_p^n and ω_q^n are independently chosen Gaussian random variables with zero means and variances chosen to satisfy constraints given below.

We would like the autocorrelation functions for $P_{ik}(t)$ and $Q_{ik}(t)$ to decay exponentially according to

$$\langle P_{ik}(0)P_{jl}(t) \rangle = P_{ikjl} \exp(-t/\tau_p), \quad (\text{B } 3)$$

$$\langle Q_{ik}(0)Q_{jl}(t) \rangle = Q_{ikjl} \exp(-t/\tau_q), \quad (\text{B } 4)$$

$$(\text{B } 5)$$

where for an isotropic system

$$P_{ikjl} = \frac{1}{10} [\delta_{ij}\delta_{kl} + \delta_{il}\delta_{jk} - \frac{2}{3}\delta_{ik}\delta_{jl}], \quad (\text{B } 6)$$

$$Q_{ikjl} = \frac{1}{6} [\delta_{ij}\delta_{kl} - \delta_{il}\delta_{jk}], \quad (\text{B } 7)$$

and τ_p and τ_q are the correlation times for the individual components of the normalized rate of strain and rate of rotation tensors. Choosing the coefficients for \widehat{P}_{ik}^n and \widehat{Q}_{ik}^n as complex random Gaussian variables (with independent real and imaginary parts), subject to the constraints

$$\langle \widehat{P}_{ik}^n \widehat{P}_{jl}^{n*} \rangle = P_{ikjl}/N, \quad (\text{B } 8)$$

$$\langle \widehat{P}_{ik}^n \widehat{P}_{jl}^n \rangle = 0, \quad (\text{B } 9)$$

$$\langle \widehat{Q}_{ik}^n \widehat{Q}_{jl}^{n*} \rangle = Q_{ikjl}/N, \quad (\text{B } 10)$$

$$\langle \widehat{Q}_{ik}^n \widehat{Q}_{jl}^n \rangle = 0, \quad (\text{B } 11)$$

satisfies (B 4) and (B 5) at $t = 0$.

In the limit $R_\lambda \rightarrow \infty$, the integral time scale (over which the dissipation and enstrophy vary) is much larger than the Kolmogorov time scale, so that we may assume $\tau_p \approx \tau_s$ and $\tau_q \approx \tau_r$, both of which are known from DNS to be $\tau_s = 2.3/\Gamma_\eta$ and $\tau_r = 7.2/\Gamma_\eta$. However, at the moderate values of R_λ corresponding to the DNS, the two time scales overlap and therefore the integral time scale must be taken into account. The modified expressions for the time correlations are given by

$$\tau_s = \frac{1}{4\langle \epsilon \rangle} \left[\sigma_{\epsilon^{1/2}}^2 \left(\frac{1}{\tau_p} + \frac{1}{\tau_{\epsilon^{1/2}}} \right)^{-1} + \langle \epsilon^{1/2} \rangle^2 \tau_p \right], \quad (\text{B } 12)$$

$$\tau_r = \frac{1}{4\langle \zeta \rangle} \left[\sigma_{\zeta^{1/2}}^2 \left(\frac{1}{\tau_q} + \frac{1}{\tau_{\zeta^{1/2}}} \right)^{-1} + \langle \zeta^{1/2} \rangle^2 \tau_q \right]. \quad (\text{B } 13)$$

Here, $\tau_{\epsilon^{1/2}}$ and $\tau_{\zeta^{1/2}}$ are the correlation times for the autocorrelations of $\epsilon^{1/2}$ and $\zeta^{1/2}$, obtained from the stochastic model for $\chi(t)$ and $\beta(t)$ discussed in Appendix A. By fitting the DNS, we obtain $\tau_p = 2.47/\Gamma_\eta$ and $\tau_q = 8.31/\Gamma_\eta$ at $R_\lambda = 47.1$, and $\tau_p = 2.47/\Gamma_\eta$ and $\tau_q = 8.50/\Gamma_\eta$ at $R_\lambda = 57.3$.

The only remaining quantities to complete the model are the frequencies ω_p and ω_q . To derive the probability density function for these quantities, we note that Fourier transform of the left-hand sides of (B 4) and (B 5) can be written as

$$\mathcal{F}\{\langle P_{ik}(0)P_{jl}(t) \rangle\} = N\langle \widehat{P}_{ik}^n \widehat{P}_{ik}^{n*} \rangle P(\omega_p), \quad (\text{B } 14)$$

$$\mathcal{F}\{\langle Q_{ik}(0)Q_{jl}(t) \rangle\} = N\langle \widehat{Q}_{ik}^n \widehat{Q}_{ik}^{n*} \rangle P(\omega_q), \quad (\text{B } 15)$$

while the right-hand sides of the same two equations become

$$\mathcal{F}\{\langle P_{ik}(0)P_{jl}(t) \rangle\} = \frac{2\tau_p P_{ikjl}}{1 + (\pi\omega_p \tau_p)^2}, \quad (\text{B } 16)$$

$$\mathcal{F}\{\langle Q_{ik}(0)Q_{jl}(t) \rangle\} = \frac{2\tau_q Q_{ikjl}}{1 + (\pi\omega_q \tau_q)^2}. \quad (\text{B } 17)$$

Equating the two relationships yields the following probability density functions for ω_p and ω_q

$$P(\omega_p) = \frac{\tau_p}{1 + (\pi\omega_p \tau_p)^2}, \quad (\text{B } 18)$$

$$P(\omega_q) = \frac{\tau_q}{1 + (\pi\omega_q \tau_q)^2}. \quad (\text{B } 19)$$

N real values of ω_p and ω_q are chosen from this distribution.

REFERENCES

- ABRAMOWITZ, M. & STEGUN, I. A. 1964 *Handbook of Mathematical Functions*. Dover.
- BALKOVSKY, E., FALKOVICH, G. & FOUXON, A. 2001 Intermittent distribution of inertial particles in turbulent flows. *Phys. Rev. Lett.* **86**, 2790–2793.
- BATCHELOR, G. K. 1967 *An Introduction to Fluid Dynamics*. Cambridge University Press.
- BRUNK, B. K., KOCH, D. L. & LION, L. W. 1997 Hydrodynamic pair diffusion in isotropic random velocity fields with application to turbulent coagulation. *Phys. Fluids* **9**, 2670–2691.
- BRUNK, B. K., KOCH, D. L. & LION, L. W. 1998 Turbulent coagulation of colloidal particles. *J. Fluid Mech.* **364**, 81–113.
- CANTWELL, B. J. 1993 On the behavior of velocity-gradient tensor invariants in direct numerical simulations of turbulence. *Phys. Fluids A* **5**, 2008–2013.
- COLLINS, L. R. & KESWANI, A. 2004 Reynolds number scaling of particle clustering in turbulent aerosols. *New J. of Phys.* **6**, 119.
- EATON, J. K. & FESSLER, J. R. 1994 Preferential concentration of particles by turbulence. *Intl J. Multiphase Flow* **20**, 169–209.
- ESWARAN, V. & POPE, S. B. 1988 An examination of forcing in direct numerical simulations of turbulence. *Comput. Fluids* **16**, 257–278.
- GARDINER, C. W. 1985 *Handbook of Stochastic Methods for Physics, Chemistry and the Natural Sciences*. Springer.
- GIRIMAJI, S. S. & POPE, S. B. 1990 A diffusion model for velocity gradients in turbulence. *Phys. Fluids A* **2**, 242–256.
- HINZE, J. O. 1975 *Turbulence*. McGraw-Hill.
- HOLTZER, G. L. & COLLINS, L. R. 2002 Relationship between the intrinsic radial distribution function for an isotropic field of particles and lower-dimensional measurements. *J. Fluid Mech.* **459**, 93–102.
- KOCH, D. L. 1990 Kinetic theory for a monodisperse gas-solid suspension. *Phys. Fluids A* **2**, 1711–1723.
- KOCH, D. L. & POPE, S. B. 2002 Coagulation-induced particle-concentration fluctuations in homogeneous, isotropic turbulence. *Phys. Fluids* **14**, 2447–2455.
- KRAICHNAN, R. H. 1970 Diffusion by a random velocity field. *Phys. Fluids* **13**, 22–31.

- McLAUGHLIN, J. B. 1994 Numerical computation of particles-turbulence interaction. *Intl J. Multiphase Flow* **20**, 211–232.
- MAXEY, M. R. 1987 The gravitational settling of aerosol particles in homogeneous turbulence and random flow fields. *J. Fluid Mech.* **174**, 441–465.
- MAXEY, M. R. & RILEY, J. J. 1983 Equation of motion for a small rigid sphere in a nonuniform flow. *Phys. Fluids* **26**, 883–889.
- POPE, S. B. 2000 *Turbulent Flows*. Cambridge University Press.
- POPE, S. B. 2002 A stochastic Lagrangian model for acceleration in turbulent flows. *Phys. Fluids* **14**, 2360–2375.
- PRATSINIS, S. E., ZHU, W. & VEMURY, S. 1996 The role of gas mixing in flame synthesis of titania powders. *Powder Technol.* **86**, 87–93.
- READE, W. C. & COLLINS, L. R. 2000a Effect of preferential concentration on turbulent collision rates. *Phys. Fluids* **12**, 2530–2540.
- READE, W. C. & COLLINS, L. R. 2000b A numerical study of the particle size distribution of an aerosol undergoing turbulent coagulation. *J. Fluid Mech.* **415**, 45–64.
- REEKS, M. W. 1991 On a kinetic equation for the transport of particles in turbulent flows. *Phys. Fluids* **3**, 446–456.
- SAFFMAN, P. G. & TURNER, J. S. 1956 On the collision of drops in turbulent clouds. *J. Fluid Mech.* **1**, 16–30.
- SAWFORD, B. L. 1991 Reynolds number effects in Lagrangian stochastic models of turbulent dispersion. *Phys. Fluids A* **3**, 1577–1586.
- SHAW, R. A. 2003 Particle–turbulence interactions in atmospheric clouds. *Annu. Rev. Fluid Mech.* **35**, 183–227.
- SQUIRES, K. D. & EATON, J. K. 1991 Preferential concentration of particles by turbulence. *Phys. Fluids A* **3**, 1169–1178.
- SUNDARAM, S. & COLLINS, L. R. 1997 Collision statistics in an isotropic particle-laden turbulent suspension. Part 1. Direct numerical simulations. *J. Fluid Mech.* **335**, 75–109.
- VOTH, G. A., LA PORTA, A., CRAWFORD, A. M., ALEXANDER, J. & BODENSCHATZ, E. 2002 Measurement of particle accelerations in fully developed turbulence. *J. Fluid Mech.* **469**, 121–160.
- WANG, L.-P., WEXLER, A. S. & ZHOU, Y. 1998 Statistical mechanical descriptions of turbulent coagulation. *Phys. Fluids* **10**, 2647–2651.
- WANG, L.-P., WEXLER, A. S. & ZHOU, Y. 2000 Statistical mechanical description and modelling of turbulent collision of inertial particles. *J. Fluid Mech.* **415**, 117–153.
- YEUNG, P. K. 2001 Lagrangian characteristics of turbulence and scalar transport in direct numerical simulations. *J. Fluid Mech.* **427**, 241–274.
- YEUNG, P. K. & POPE, S. B. 1989 Lagrangian statistics from direct numerical simulations of isotropic turbulence. *J. Fluid Mech.* **207**, 531–586.
- ZACHNIK, L. I. & ALIPCHENKOV, V. M. 2003 Pair dispersion and preferential concentration of particles in isotropic turbulence. *Phys. Fluids* **15**, 1776–1787.
- ZHOU, Y., WEXLER, A. S. & WANG, L.-P. 2001 Modelling turbulent collision of bidisperse inertial particles. *J. Fluid Mech.* **433**, 77–104.